*Accepted for Publication*

# Seismic coupling for the Aegean - Anatolian region

Federica Sparacino[1], Bruno G. Galuzzi[2], Mimmo Palano[1*], Margarita Segou[3], Claudio Chiarabba[4]

[1] Istituto Nazionale di Geofisica e Vulcanologia, Osservatorio Etneo - Sezione di Catania, Catania, Italy

[2] Department of Biotechnology and Biosciences, University of Milan-Bicocca, Milan, Italy

[3] British Geological Survey, The Lyell Center, Research Avenue South, EH14 4AP, Edinburgh, UK

[4] Istituto Nazionale di Geofisica e Vulcanologia, Osservatorio Nazionale Terremoti, Roma, Italy

[*]***Corresponding author*:**

Mimmo Palano

Istituto Nazionale di Geofisica e Vulcanologia, Osservatorio Etneo - Sezione di Catania,

P.zza Roma 2, I-95123 Catania (Italy)

Phone: +39 0957165800

Email: mimmo.palano@.ingv.it

**Abstract**

Seismic coupling helps define how large the earthquake potential of a region is, as well as the presence of asperities along plate zones. This work seeks to provide an improved picture of the seismic coupling for the Aegean-Anatolian region by taking advantage of extensive seismic and geodetic datasets. To estimate coupling, we compiled a series of by-products that are specific ingredients also for seismic hazard studies. With these by-products, we found that the seismogenic thickness is thinner (10-15 km) or thicker (20 to 30 km) to the east and to the west, respectively and even deeper along the Hellenic subduction zone. The *b-value* ranges between 0.9 and 1.1 for the entire area with high values concentrated at locations of Late Miocene to -recent volcanism whereas low *b-values* (<0.8) concentrate along most of the Northern Anatolian fault zone that may suggests stress accumulation. Seismic coupling is low (<35%) or intermediate (35% - 70%) in most of the area, while the Karliova triple junction, on a N-S-oriented belt along the boundary between western and central Anatolia, and the southeastern Peloponnese are fully coupled, suggesting a full seismic release of the entire deformation budget. An intermediate value of seismic coupling is observed for the eastern and central segments of the Northern and Eastern Anatolian Fault zones, for part of the Hellenic volcanic arc, the Kefalonia Transform Fault and the Corinth gulf active faults. Considering historical earthquake data, these intermediate coupling values indicate either aseismic deformation or catalog incompleteness. Furthermore, the time period since large magnitude earthquakes clearly raises the possibility of impending earthquakes on the Northern and Eastern Anatolian Fault zones. A broad seismic gap is evidenced along the Hellenic subduction zone, because of the reduced coupling and the absence of ~M8 earthquakes in the last 700 years, at least. We conclude that in most of the central Aegean Sea aseismic deformation prevails as suggested by the small value of coupling and the modest seismic release over the last millennium.

**Keywords:** geodetic and seismic moment-rates, seismic coupling, seismic hazard, seismogenic thickness, b-value, Aegean-Anatolia

## 1. Introduction

The remarkable increase of GNSS-based networks has enabled an improved focus on geodetic moment-rates estimation in all tectonic regions worldwide (e.g. Ward, 1998; Pancha et al., 2006; Mazzotti et al., 2011; Scholz and Campos, 2012; Déprez, et al., 2013; Métois et al., 2013; D'Agostino, 2014; Carafa et al., 2017; Palano et al., 2018). Since the pioneering work of Kostrov (1974), understanding how strong the coupling between deformation and earthquake generation is, remains a challenge in seismology. Coupling estimates are difficult especially in subduction zones, partly because of their high deformation rate (Ruff and Kanamori, 1980; Uyeda, 1982; Scholz and Campos, 2012). Furthermore, the amount of crustal strain released by earthquakes reflects the rate of long-term tectonic deformation only partially. Despite the variety of methods for estimating seismic and geodetic moment-rates, the results do enable to distinguish regions where the total deformation-rate budget is entirely released by seismicity (e.g. Mazzotti et al., 2011; Pancha et al., 2006; D'Agostino, 2014; Sparacino et al., 2020), from those whose excess deformation, is potentially accommodated by other processes, such as aseismic slip, or strain accumulation related to impending large earthquakes (Masson et al., 2005; Palano et al., 2018, 2020; Déprez, et al., 2013). Seismic coupling is therefore a key parameter to assess how large the earthquake potential is in any region. Earthquake asperities correlate with areas of high coupling, but their persistence over different seismic cycles may vary according to stress accumulation (e.g. Corbi et al., 2017).

The Aegean and Anatolian microplates is affected by the highest deformation region of the Mediterranean (Figure 1), with complex tectonics leading to many large magnitude earthquakes in the past. The seismic and the associated tsunami hazard are the highest in Europe (e.g. Shaw and Jackson, 2010; Giardini et al., 2014; TSUMAPS, http://www.tsumaps-neam.eu). The first estimations of the seismic coupling for selected regions conducted by Jackson and McKenzie (1988), Papazachos and Kiratzi (1996), Ward (1998), Laigle et al. (2002), Jenny et al. (2004), Rontogianni (2010), Vernant et al. (2014) and Chousianitis et al. (2015), still leave many open questions. Despite the copious datasets and different parameterization and/or assumptions, the aforementioned studies only identified a few regions where the estimated geodetic/tectonic moment-rate is released purely by seismic activity, such as the Cephalonia Transform Fault (central Ionian Sea) and the westernmost branch of the North Anatolian fault, in the North Aegean Trough. Furthermore, the remaining part of central and northern Greece is believed to deform in aseismic mode (Rontogianni, 2010; Chousianitis et al., 2015). The behavior of the Hellenic subduction zone is widely debated with contrasting results, ranging from fully coupled (Ganas and Parsons, 2009) to various degrees of uncoupled deformation (e.g. Papazachos and Kiratzi, 1996; Scholz and Campos, 2012; Apel, 2011; Vernant et al., 2014 and references therein). In Anatolia, the first estimation of seismic coupling (Ward, 1998) concluded that the observed deformation is largely aseismic. Since then, no other estimations have been performed, despite its high seismic hazard (e.g. Bohnhoff et al., 2016 and references therein).

The contrasting results for the Aegean region, coupled with the lack of updated and robust estimation for the Anatolian region, call for a re-examination of the degree of coupling for this broader zone of the Nubia-Eurasia margin. Previous efforts were partially limited by the strong heterogeneity and granularity of information (either seismic or geodetic) available for the entire region. Therefore, our first step in acquiring a consistent estimate of the coupling is to compute uniform and homogeneous ingredients by using and merging high quality geodetic and seismic data. Our approach estimate moment-rates and seismic coupling on 2° x 2° square cells with a 75% overlap and does not require an a priori zonation, that could be sometimes subjective. The compilation of seismicity records from existing catalogs (either historical or instrumental) has been done with the aim of minimizing the impact of the large heterogeneities of available records (e.g. spatial coverage of each catalog, duplicated events, magnitude determination). We therefore compute input parameters for the coupling estimation, such as the maximum expected magnitude, the seismogenic thickness and the coefficients of the Gutenberg and Richter (1956) frequency-magnitude distribution relation, as homogeneously as possible for the entire area. In addition, based on an extensive combination of recent GNSS velocities integrated with those reported in previous works, we compiled a dense velocity field that is essential for deriving the geodetic moment-rates. Finally, the seismic coupling estimation enables characterizing the crustal deformation modality (seismic versus aseismic), as well as identifying potential seismic cycle gaps over the entire region, thereby providing additional constraints on modern seismic hazard estimates.

## 2. Background

The Aegean-Anatolian region, located in the collision zone between the African, Arabian and Eurasian plates (Figure 1), undergoes a series of diverse and complex long-lasting tectonic processes (e.g. McKenzie et al., 1970, Sengör and Yılmaz, 1981). Since the Jurassic, the convergence between Africa and Eurasia plates has led to the development of a circum-mediterranean Alpine belt (van Hinsbergen et al., 2020 and references therein), with different partially independent segments. Among these, the Hellenides were divided into northern and southern segments (Doutsos et al., 2006; Papanikolau, 2010). The northern segments remained trapped in the continental collision (occurring at rates of ~5-10 mm/yr) against the Apulian foreland (a northern promontory of the African plate; Figure 1). At the margin of the southern segment, rapid subduction of the African plate beneath western Turkey and the Aegean regions developed (with current rates of ~40 mm/yr; Reilinger et al., 2006), forming

the Hellenic subduction zone (e.g. Papanikolau, 2010; Jolivet and Brun, 2010). Such a rapid subduction with slab roll-back caused the extension of the continental crust and volcanism in the overlying Aegean region (Koukouvelas and Aydin 2002; Kokkalas et al. 2006; Jolivet et al., 2013).

After the Late Eocene (~35 Ma), the Arabian continental margin, facilitated by negative buoyancy, moved northward and under-thrusted the Eurasian plate (Jolivet and Faccenna, 2000), while the onset of the continental crustal thickening began in the Late Oligocene (~25 Ma; Mouthereau et al. 2012. The continuing northward migration of the Arabian with respect to the stable Eurasia plate resulted in crustal shortening and the thickening of the Eastern Anatolian Plateau as well as, after the Late Miocene, widespread volcanism (Figure 1) along the southern sector of the Central Anatolian Plateau (e.g. Sengor et al., 2003). After the Early Pliocene, the Arabia-Eurasia collision was arranged by the westward extrusion of a continental block along two major strike-slip faults, the North and East Anatolian fault zones, respectively (NAFZ and EAFZ; e.g. Sengor et al., 2005; Bulut et al., 2012). The EAFZ is a left-lateral fault system extending from the Karliova triple junction, where it joins the NAFZ, toward the southwest for about 600 km to the Hatay triple junction (Mahmoud et al., 2013). NAFZ is a right-lateral fault system extending for ~1200 km from the Karliova triple junction in the east to the northern Aegean Sea in the west (Bohnhoff et al., 2016). NAFZ marks a narrow fault zone along its eastern and central parts, while it branches into two or three sub-parallel strands along its western portion (e.g. Marmara Sea and North Aegean Trough; Koukouvelas and Aydin, 2002).

The Hellenic subduction zone (Figure 1) is confined between the right-lateral Cefalonia transform fault (CTF, hereinafter) to the west and the Pliny-Strabo shear zone (PSSZ, hereinafter), to the east (Kokkalas et al. 2006). The southwest-trending CTF marks the transition between the westernmost termination of the Hellenic subduction and the continental collision zone (between northern Hellenides and the Apulian platform) to the north (Louvari et al., 1999 and references therein). The PSSZ is a left-lateral tectonic belt characterized by heterogeneous tectonic features, which has recently been interpreted as the surface expression of a tearing process between the Aegean lithosphere in the NW and the African lithosphere in the SE (Özbakır et al., 2013; Howell et al., 2017). Eastward of PSSZ, the Cyprian Arc arranges the transition from the Hellenic subduction to the continental collision between the Anatolian plate in the north and the Nubian plate in the south (Wdowinski et al., 2006).

In the last three decades, several authors have focused on the seismic coupling for the Aegean-Anatolian region, using different geologic, geodetic and seismic datasets and adopting different formulations (see Table 1 for a summary). An early estimation was done by Jackson and McKenzie (1988), who inferred a substantial aseismic behavior of the Hellenic subduction zone. Similar results were obtained later by Vernant et al. (2014), who inferred a seismic coupling of 10% along the entire Hellenic subduction interface and a 5700-8300 year recurrence time for 365 CE-type Crete events. Moreover, Ward (1998) estimated a seismic coupling of 66% and 22% for the Aegean and the Anatolian regions, respectively, while Laigle et al. (2002) suggested that in the Ionian Islands region, the subduction zone is fully coupled. Jenny et al. (2004) inferred moderate to large seismic coupling along the CTF and the western segments of NAFZ, and significant uncoupling (up to 90%) along the Southern Aegean Sea and the Hellenic subduction zone. Rontogianni (2010) observed a large seismic strain deficit for most of Greece, therefore highlighting the possibility of future large earthquakes to fill the deformation deficit. Chousianitis et al. (2015) observed that in the central Ionian Sea, the geodetic strain is fully seismically released, while in other sectors of Greece the geodesy-based moment-rates were at least 2 times higher than the earthquake-based ones, evidencing a possible seismic catalog incompleteness (e.g. western Peloponnese, Epirus, North-western Aegean Sea) or important aseismic deformation (e.g. Gulf of Corinth).

## 3. Data

3.1 Seismic catalogs

The occurrence of several large earthquakes in the Aegean-Anatolian region is well-documented in remarkably complete historical records and written sources (Bohnhoff et al., 2016). By taking into account both the SHEEC and SHARE-CET catalogs (https://www.emidius.eu/SHEEC; Stucchi et al., 2013; Grünthal et al. 2013; Papadopoulos, 2011), we compiled a catalog of 678 historical earthquakes (HE, hereinafter) occurring in the investigated area during the 1003 - 1903 period and with estimated moment magnitude $M_w \geq 5$. Historical seismicity is widespread over the whole investigated area (Figure 2), with the strongest earthquakes ($M \geq 7$) mainly concentrated along the western and eastern sectors of NAFZ, the EAFZ and along the Hellenic Trench (see also Table S1 in Supplementary material). The largest earthquake occurred in on August 8, 1303 ($M_w$ 8.26, Stucchi et al., 2013), with the estimated epicenter located to the east of Crete.

We also compiled a catalog of instrumental seismicity (IE, hereinafter) by merging the records reported in the following online catalogs (see Supplementary material for more information):

- National catalog for Greece (Figure S1) managed by the "Institute of Geodynamics-National Observatory of Athens" (http://www.gein.noa.gr/en/seismicity/earthquake-catalogs);
- National catalog for Turkey (Figure S2) managed by the "Kandilli Observatory and Earthquake Research Institute of Bogazici University" (http://www.koeri.boun.edu.tr/sismo/2/earthquake-catalog);
- ISC catalog (Figure S3) (http://www.isc.ac.uk);
- ISC-GEM catalog (Figure S4) (http://www.isc.ac.uk/iscgem/index.php);

The resulting catalog has a time span from August 1903 to December 2020 for a total amount of 864,298 events, with ranges in magnitude and depth from 1.5 to 7.8 and from 0 to 50 km, respectively. The largest earthquakes reported in the catalog (Figure 2) occurred along the central (i.e., the 1944 $M_w$ 7.6 Ulumescit event and the 1943 $M_w$ 7.5 Comert-Ilgaz one) and eastern sectors of NAFZ (i.e., the 1939 $M_w$ 7.8 Erzincan event), and in the southern Aegean region (i.e. the 1956 $M_w$ 7.7 Amorgos event).

3.3 GNSS data

We analyzed an extensive GNSS dataset by collecting raw observations from SOPAC (ftp://garner.ucsd.edu/pub), EUREF (https://www.epncb.oma.be), NOAA (ftp://alt.ngs.noaa.gov/cors) and UNAVCO (ftp://data-out.unavco.org). The GNSS phase observations were processed by using the GAMIT/GLOBK 10.7 software (Herring et al., 2018) following the approach described in Palano et al. (2020) in order to estimate a consistent set of positions and velocities in a fixed Eurasian reference frame (Palano et al., 2017). To improve the spatial density of the geodetic velocity field over the study area, we integrated our solutions with those reported in recent literature (Nocquet, 2012; Tatar et al., 2012; Aktŭg et al., 2013; Tiryakioğlu et al., 2013; Vernant et al., 2014; Chousianitis et al., 2015; Metois et al., 2015; England et al., 2016; D'Agostino et al., 2020) by solving for Helmert transformation parameters that minimize the differences between velocities at common sites (e.g. Herring et al., 2018). We removed all sites having a formal error greater than 1.5 mm/yr (e.g. 3 times larger the average error of the whole dataset) in their velocity; all the removed sites correspond to literature solutions and account for less than 5% of the whole dataset. The final velocity field is reported in Figure 3a and Table S2.

We estimated the horizontal strain-rates using the method of Shen et al. (2015), which allows us to model the horizontal velocity gradients on a regularly spaced grid by means of a least squares inversion (see Supplementary Material). To estimate strain-rates along the Hellenic and the Cyprian subduction zones, we defined a composite velocity field (Figure S5) given by our final velocity field and by the one, computed on a 0.5° x 0.5° grid, from the expected motion of the Nubian plate with respect to the Eurasian one. The subduction interface by Basili et al. (2013) is used to define the northern

boundary of the Nubian velocity field. Our final strain-rate field is reported in Figure 3b (see also Figure S6 and the associated text in the Supplementary Material for additional details).

## 4. Methods and parameters definition

We present the approaches and the mathematical formulation for intermediate parameters and seismic and geodetic moment-rates computation. Subsequently, we discuss how these parameters have been estimated and their relative impact on the moment-rates computation.

### *4.1 Seismic source zonation and cell size definition*

The seismic and geodetic moment-rates comparison, as well as seismic hazard, are usually performed on seismically homogeneous source zones that are defined on the basis of tectonic, geological and seismic considerations (e.g. Mazzotti et al., 2011, Erdik et al., 1999). Available seismic zonations for the study area (e.g. Giardini et al., 2013 and references therein) consist of several small size sources along main active faults. Most of the seismic sources are not fully covered by GNSS stations, so that the strain-rates information can only be derived from the velocity interpolation. To overcome such limitations and enable a common estimation for different tectonic settings without the need for a priori tectonic information, we adopt a spatially extended parameterization for the seismic sources. We divided the study area into a regular grid with square cells of 2° x 2° and a 75% overlap. The chosen cell size is consistent with the rupture length of a M=8 earthquake (Wells and Coppersmith, 1994), and the 75% overlap results in a 0.5° x 0.5° pseudo-grid, matching the size of the seismic source zones (Giardini et al., 2013).

### *4.2 Methods for moment-rates estimation*

For each computational cell, the seismic moment-rate ( $\dot{M}_{seis}$ ) has been calculated by adopting a truncated cumulative Gutenberg-Richter distribution (Hyndman and Weichert, 1983):

$$\dot{M}_{seis} = \varphi \frac{b}{(c-b)} 10^{[(c-b)M_{\max}+a+d]}, \qquad (1)$$

where:

- $M_{max}$ is the magnitude of the largest earthquake that could occur within the cell.
- $\varphi$ is an asymmetric correction for the stochastic magnitude-moment relation.
- $c$ and $d$ are the coefficients of the moment magnitude ($M$) - seismic scalar moment ($M_{seis}$) relation:

$$logM_{seis} = cM + d\ , \quad (2)$$

- $a$ and $b$ represent the measure of the annual level of seismicity and the ratio between the number of small and large earthquakes, respectively, of the Gutenberg and Richter (1956) recurrence relation:

$$logN(M) = a - bM \quad , \quad (3)$$

and are strictly related to moderate magnitudes of the catalog. $N(M)$ is the cumulative number of earthquakes with magnitude $M$ and larger for each cell.

We assumed $\varphi$ = 1.27, reflecting an average error of 0.2 on magnitudes (Hyndman and Weichert, 1983), and $c$ = 1.5 and $d$ = 9.1 for $M_{seis}$ in N m (Hanks and Kanamori, 1979), while the $a$, $b$

and $M_{max}$ values have been estimated for each cell on the basis of available historical (HE) and instrumental (IE) seismic catalogs. Our IE catalog refers to different scales (see Supplementary material), which should ideally be converted into moment magnitude ($M_w$) before computing (eq. 3). However, we prefer to convert all earthquake magnitudes directly into scalar moments, because in any case, both estimations will always suffer from substantial uncertainties.

The scalar seismic moment-rate can also be estimated by adopting the moment summation approach of Kostrov (1974):

$$\dot{M}_{seis} = \frac{1}{\Delta T}\sum_{n=1}^{N} M_{seis}^{(n)} \qquad (4)$$

where $N$ is the number of events occurring during a given time interval $\Delta T$ in the volume $A \cdot H_s$ (with $A$, the surface area and $H_s$, the seismogenic thickness), $M_{seis}$ is the scalar seismic moment of the *n-th* earthquake from the $N$ total earthquakes. We mainly focused on seismic moment-rate estimations from the truncated Gutenberg-Richter distribution. However, in order to test sensitivity, we performed additional computations by taking into account the Kostrov summation approach and using a catalog (M5E hereinafter) including all earthquakes with M≥5 reported in the instrumental (IE) and the historical (HE) ones.

Concerning the geodetic moment-rate, slightly different formulations relating the surface strain-rates to scalar moment-rates over a seismic volume have been proposed in literature (see Pancha et al., 2006 for an overview). Here we adopted the Savage and Simpson (1997) formulation, which derive from the generic one proposed by Kostrov (1974) and allows to consider strains in multiple directions:

$$\dot{M}_{geod} = 2\mu H_s A[Max(|\varepsilon_{Hmax}|, |\varepsilon_{hmin}|, |\varepsilon_{Hmax} + \varepsilon_{hmin}|)] \ , \qquad (5)$$

where $\mu$ is the shear modulus of the crust, $H_s$ is the seismogenic thickness over which strains accumulate and its elastic part releases in earthquakes, $A$ is the surface area of the selected cell, $\varepsilon_{H\max}$ and $\varepsilon_{h\min}$ are the principal horizontal strain-rates and *Max* is a function returning the largest of the arguments. We set $\mu = 3.0 \cdot 10^{10}$ N m$^{-2}$ (typical value of average crustal rocks; Turcotte and Schubert, 2002), while the principal horizontal strain-rates have been estimated for each cell by taking into account the GNSS velocity field.

## 5. Parameters estimation and results

### *5.1 $M_{max}$ estimation*

Different approaches can be used to estimate the $M_{max}$ value of a given region. In long-term hazard models, the standard practice is to add 0.5 to the magnitude of the largest earthquake reported in the historical catalog (Kijko and Graham, 1998), but this approach is very limited in those areas with no significant historical record. $M_{max}$ can also be estimated by adopting a law-scale relating magnitude to fault dimension (Wells and Coppersmith, 1994), but several issues on fault segmentation arise.

We estimated $M_{max}$ by using the toolbox developed by Kijko and Singh (2011), which uses 12 different statistical procedures. The benefit of using this toolbox is that it provides reliable results under different data restrictions (magnitude of completeness and temporal length of the catalogs, magnitude distribution and uncertainties, number of earthquakes, etc.). We used as input the M5E catalog, assuming an average error of 0.2 on magnitude values. $M_{max}$ values have been estimated by considering the same grid-knots of the other computations, where the cell's size has been enlarged (3° x 3°) in order to take the location uncertainties of historical earthquakes into account. For each cell, among the 12 estimated $M_{max}$ values, we chose the one associated with the smallest uncertainty.

The pattern of $M_{max}$ (Figure 7a) is characterized by values ranging from 6.0 to 8.5. The highest values (~8.5) have been estimated for a large sector of the Aegean region, mainly because of the devastating $M_w$ 8.26 1303 Crete earthquake. Magnitude values within the 7.5-8.0 range were estimated for the central and easternmost sector of NAFZ and along the Hatay triple junction, the PSSZ and southern Peloponnese. Values within the 7.0-7.5 range were estimated for the western and eastern sectors of NAFZ, the eastern sector of EAFZ, western Turkey and central and eastern Greece. Values smaller than 7.0 characterize the remaining areas with lowest values (~6.0) in south-central Turkey. Estimated uncertainties (Figure 7b) range from 0.25 to 0.48, with largest values found in southern Greece and eastern Turkey (see also Table S3 in the supplementary material).

*5.2 Coefficients of the Gutenberg-Richter recurrence relation*

The coefficients *a* and *b* of the Gutenberg-Richter recurrence relation (eq. 3) express the frequency vs. magnitude distribution of earthquakes over a given space-time interval. The *a-value* corresponds to the seismic-rate of the region, while the *b-value* describes the relative frequency of large vs small events, regardless of population size. Typical values range in the interval 0.6-1.4 with a global mean of ~1.0 (Frohlich and Davis, 1993). The *b-value* depends on factors, such as material heterogeneity (Mogi, 1962) or applied shear stress (Scholz, 1968): low values, that is a high proportion of major earthquakes, are inferred to indicate areas of crustal homogeneity and high stress, whereas, high values indicate crustal heterogeneity and low stress (Mogi, 1962; Mori and Abercombie, 1997).

We estimate these coefficients within the 2° x 2°, 75% overlap grid. Computation has been limited to cells with at least 40 earthquakes, by using the IE catalog and two different approaches: the maximum likelihood estimation (MLE; Weichert, 1980) and the robust fitting method (RFM; Han et al., 2015). Such a double computation has been performed in order to check the robustness of achieved results.

The aforesaid parameters are estimated as:

$$b = \frac{1}{ln\,(10)\cdot(\mu_M - M_{thresh})} \quad , \quad (6)$$

$$a = log_{10}\frac{M}{\Delta T} + b \cdot M_{thresh} \quad , \quad (7)$$

where $M$ are the magnitudes of the analyzed dataset, $\mu_M$ is the sampling average of the magnitudes, and $M_{thresh}$ is the threshold magnitude which usually corresponds to the magnitude of completeness ($M_c$) of the catalog, i.e. the value below which the number of detected earthquakes is considered incomplete (Rydelek and Sacks, 1989; Wiemer and Wyss 2000; Han et al., 2015). The parameter $\Delta T$ is the temporal window covered by the catalog.

The *a-* and *b-value* distribution varies significantly over the area (see also Table S3 in the supplementary material). The *a-value* ranges between 4.67-7.85 (Figure 5a) and 3.28-7.98 (Figure 5c) from MLE and RFM, respectively. Values smaller than 5 can be observed mainly along the northern border of the computation region, especially considering the MLE results, while similar ones coming from RFM are also concentrated along the easternmost sector of the NAFZ. Values larger than 6.5 define, for both approaches, a near continuous region including western Turkey and Greece, with the largest values (>7.5) along the PSSZ.

The *b-value* falls in the range of 0.66-1.37 (Figure 5b) and 0.50-1.26 (Figure 5d) from MLE and RFM, respectively, showing a general agreement with small differences in the north-eastern sector of the study area where RFM suggests smaller *b-values*. For most of the study area, values range within the 0.9-1.1 interval, while small patches with values > 1.1 are observed for the southern Aegean Sea and in south-eastern Turkey. The RFM approach results in larger *b-values* also for PSSZ.

Another computed parameter is *Mc*, i.e. the magnitude of completeness of the catalog. Although the *Mc* values are computed from both methods, since the RFM approach is less sensitive to *Mc* values, we refer only to the values estimated by the MLE approach. For most of Turkey, *Mc* is ~2.5 on average (Figure 6), while in a large area of its western site, *Mc* ranges in the 3.3-3.6 interval. Regarding the Greek region, *Mc* is ~2.6 on average for the central sector, while values of ~2.9 characterize north-western Greek and most of the Aegean Sea; *Mc* values increase southward approaching the Mediterranean offshore.

*5.3 Seismogenic thickness*

The thickness of the seismogenic layer is a key parameter for seismic hazard since it helps constrain the maximum depth of faulting and the potential earthquake magnitude (Nazareth and Hauksson, 2004). Previous computation of SCC in the study area adopted uniform and fixed values of 15 km (e.g. Jenny et al., 2004; Ward,1988; Rontogianni, 2010; Chousianitis et al., 2015). A valid approach to estimate the thickness is given by the seismicity cut-off at depth, i.e., the depth above which a given percentage (e.g. 90%, Miller and Furlong, 1988; 95%, Williams, 1996; Chiarabba and De Gori 2016) of the hypocenters or the moment release within a depth column occurs. Although the choice of this percentage is related to the amount and quality of locations, the 90% value is widely used in seismic hazard (e.g. Nazareth and Hauksson, 2004; Pancha et al., 2006; Stein, 2008; Smith-Konter et al., 2011). Here, we adopt the 90% criterion to also balance between regions with different amounts of data. We divided the study area into a regular grid with square cells (0.5° x 0.5°), with a 50% overlap and used the IE catalog. We discarded all the events with fixed depth and considered only the cells containing at least 30 events. Since earthquakes in our catalog do not report hypocentral vertical errors, we applied a bootstrap statistic with replacement to account for depth uncertainty in the seismogenic thickness estimation (see Supplementary material). Moreover, to test results sensitivity we performed additional estimations by excluding all earthquakes with focal depths larger than 30, 35 and 40 km (Figure S7 of the supplementary material), respectively. Seismogenic thickness values are similar for the eastern sector and the northern portion of the western one, while results along the Hellenic subduction zone show some differences.

In particular, along the subduction zone differences larger than 3 km, confined to a narrow belt, arise from the comparison between ST30 and ST35, while differences larger than 4.5 km over a wider region, result from the comparison between ST35 and ST40 (Figure S7). These results highlight the dependence of seismogenic thickness estimations on the deep seismicity related to the subducting plate. Here we refer to the ST35 results (Figure 4) marking two well-defined regions. The eastern region, mainly in Turkey, is characterized by seismogenic thickness ranging in the 10-15 km interval, while the western region, characterized by values ranging between 20-30 km, with the highest values along the Hellenic subduction zone. Values larger than 32 km are found offshore. The well-defined boundary between the eastern and the western sectors mirrors the one related to the *Mc* values (Figure 6), suggesting a possible sensitivity of seismogenic thickness values to different earthquake magnitude ranges in IE. To verify such a hypothesis, we performed an additional computation by taking into account all events with M>3 (see Figure S8 in the supplementary material). In these new results the well-marked boundary is always visible, therefore attesting to the robustness of our previous estimations.

*5.4 Moment-rates*

The estimated moment-rates are reported in Figure 8 (see also Table S3 in the supplementary material). Given the overall wide range of values, we simply refer to low ($< 1.0 \times 10^{18}$ N·m yr$^{-1}$), intermediate ($1.0 \times 10^{18}$ - $7.0 \times 10^{18}$ N·m yr$^{-1}$) and high ($> 7.0 \times 10^{18}$ N·m yr$^{-1}$) moment-rates values.

The seismic moment-rates estimated according to (eq. 1) are reported in Figure 8a and range in the interval $8.2 \times 10^{15}$ - $9.8 \times 10^{18}$ N·m $yr^{-1}$. Low values are concentrated in most of the study area, especially on its eastern and northern sectors, characterizing large segments of the EAFZ and the NAFZ. Intermediate values are found for southwestern Turkey and the majority of locations in Greece, whereas high values are found only along the southern termination of the PSSZ and in western and central Peloponnese, this latter being partially biased by the smearing in computation from the high seismic release of adjacent areas.

As above mentioned, the seismic moment-rates were also estimated by using the summation approach (eq. 4) and achieved values range in the interval $5.3 \times 10^{15}$ - $8.6 \times 10^{18}$ N·m $yr^{-1}$ (Figure 8b). We find that our study area is characterized by low moment-rate values, whereas cells with intermediate and high values concentrate along the central NAFZ and on the southeastern side of the Hellenic subduction zone.

Results coming from both approaches are fairly similar (the ratio between the two estimates range from 0.1 to 3) for most of the investigated area, therefore providing robust estimations on upper/lower boundaries of moment-rates. Some cells with larger ratios are found in central and eastern Turkey with differences mainly related to the different assumptions. The Kostrov approach (eq. 4) simply normalizes the cumulative estimated moments for the recorded events by the temporal duration of the catalog. As a result, this method is closely dependent on i) the length of the catalog, and ii) the possible lack of large earthquakes (with high recurrence rate compared to the catalog duration). Conversely, the truncated cumulative Gutenberg-Richter distribution approach (eq. 1) takes into account the incompleteness of the catalogue using the magnitude distribution of the events through the estimate of the *b-value*, and therefore it is insensitive to the duration of the observation period. The inspection of the temporal length of the M5E catalog (i.e. the catalog including all historical and instrumental M>5 earthquakes) for each computational cell (Figure 9a) reveals that the average duration is ~770 years with ~62% of the cells above this value and only ~10% with a duration less than 400 years. Cells having such a temporally short catalog are those in a large sector of central Turkey, which featured two large earthquakes in the last century (e.g. the 1944 $M_w$ 7.6 Ulumescit and the 1943 $M_w$ 7.5 Comert-Ilgaz events).

These observations suggest that the estimates coming from (eq. 1) and (eq. 4) match for cells with catalog duration of at least 400 years, whereas for cells with smaller time span catalogs, like those located in central Turkey, results from (eq. 4) are overestimated. A duration of 400 years can be considered as the minimal temporal length to reasonably capture the statistical long-term behavior of seismicity over the study area.

The geodetic moment-rates estimated according to (eq. 5) are reported in Figure 8c and range in the interval $5.8 \times 10^{17}$ - $1.5 \times 10^{19}$ N·m $yr^{-1}$. Low values are mostly concentrated in the area of southern central Turkey and Cyprus, while moderate values are found in the rest of the area. High moment-rates are present only in the Hellenic subduction zone in northwest Greece, and in the region including the CTF, the gulfs of Patras, Corinth and the Peloponnese (Figure 8c).

## 6. Discussion

In this section, we first review and discuss the byproducts of the geodetic and seismic moment-rates computation, which are significant for characterizing the seismicity and general features of the area. We then present and discuss the moment-rates and the seismic coupling of the broad area.

### *6.1 Geodetic and seismic byproducts*

The updated GNSS field provides very dense information on the present-day kinematics of the study area (Figure 3a). In general agreement with previous studies (e.g. Reilinger et al., 2006; Le Pichon and Kreemer, 2010; Pérouse et al., 2012; England et al., 2016), the most significant feature is the near-

circular counterclockwise motion of the Aegean-Anatolian region with respect to Eurasia. Although GNSS velocities appear relatively described by such a counterclockwise motion, they are not consistent with a single rigid body rotation, since they show increasing values from eastern Anatolia (~20 mm/yr) to the Aegean area (~30 mm/yr). The strain-rate field (Figure 3b) clearly depicts the strike-slip behavior of NAFZ with extensional axes progressively rotating from E-W to N-S, respectively moving from the eastern NAFZ toward the northern Aegean Sea. Such a rotation is coupled with an increase of the extension, especially along the western NAFZ and the northern Aegean Sea, the latter extensional component marked by the Aegean Trough before we reach continental Greece with a maximum of ~100 nanostrain/yr on the Gulf of Corinth, with a purely extensional environment. This diffuse N-S extension spreads also over western Turkey and eastern Aegean Sea with values up to ~95 nanostrain/yr. Central-southeastern Anatolia is characterized by a less pronounced extension with values up to 50 nanostrain/yr for the EAFZ.

The Hellenic subduction zone is characterized by a pure compression up to 160 nanostrain/yr, passing toward a strike-slip behavior along its edges at CTF and PSSZ. The compressional component progressively vanishes eastward along the Cyprian arc, approaching the Hatay triple junction and the Dead Sea fault system. Overall, our strain-rate field agrees with previous GNSS- and InSAr-based estimations (Le Pichon and Kreemer, 2010; Pérouse et al., 2012; Weiss et al., 2020), but defines the main tectonic features and kinematics of the entire Aegean-Anatolian region with higher resolution.

The *Mc* parameter is generally used to characterize the general efficacy of seismic monitoring of a given area and the completeness of seismic bulletins. The *Mc* spatial pattern over the study area (Figure 6) is heterogeneous and ranges in the 2.3-3.6 interval; it allows identifying some regions (e.g. all cells with *Mc*>3.0) where densification of seismic networks would help reduce the magnitude detection, ensuring a uniform monitoring.

Another relevant byproduct is the *b-value* of the Gutenberg-Richter recurrence relation. Our results concur well for the Anatolian region with the ones reported in Kalyoncuoglu (2007). For most of the study area, our estimated values fall in the 0.9-1.1 interval. Small patches with values greater than 1.1 can be observed for the southern Aegean Sea and in south-eastern Turkey, in close correspondence of the Late Miocene-recent volcanism, highlighting a heterogeneous crust with an extraordinarily high number of small earthquakes in a low stress context (McNutt, 2005). A relative increase of the *b-value* east of Creete may suggest a tendency to low stress accumulation along this segment of the subduction zone. Patches characterized by values lower than 0.8 concentrate along most of the NAFZ, suggesting a general tendency for stress accumulation. A systematic *b-value* increase along the fault evidences an inverse correlation with the decreasing age/maturity of the fault system according to Bohnhoff et al. (2016).

A continuous map of the thickness of the seismogenic layer beneath the Aegean-Anatolian region (Figure 4 and Table S4 in the supplementary material) reveals a high variability, with a thinner sector to the east, mainly including Turkey (10-15 km) and a thicker sector to the west (20 to 30 km), with the larger values (>32 km) along the Hellenic subduction zone. The estimates are in agreement with the few ones reported in past studies, using local microseismicity across active faults such as NAFZ (Grosser et al., 1998; Bulut and Aktar, 2007; Yolsal-Çevikbilen et al., 2012). The base of the seismogenic layer broadly coincides with the brittle-ductile transition where little-to-no earthquakes are commonly expected (e.g. Scholz, 1998). Theoretical crustal strength envelopes based on power law rheology suggest that the brittle-ductile transition depth should correlate with strain-rate and anti-correlate with heat flow (Sibson, 1984). In other words, thinner brittle crust should be weaker and may be expected to deform more rapidly and thus have a higher strain-rate. In addition, thinner seismogenic layers generally imply higher surface heat flow and hotter geothermal gradients. From the visual comparison between the seismogenic thickness (Figure 4) and the geodetic strain-rate (Figure 3b), no significant correlation is evident. The surface heat flux measurements over the study area concentrated

in a few zones and do not provide an even regional coverage (Artemieva and Shulgin, 2019). Besides such a limitation, the seismogenic thickness inversely correlates with the surface heat flow (Chamorro et al., 2014; Artemieva and Shulgin, 2019) for most of Turkey; conversely, they fully correlated on western Turkey and the Aegean regions, where high heat flow values are expected because of the ongoing subduction process. In cases of poor information on crustal heat flux, our results could be of help to localize specific regions where high temperature can be expected.

Another relevant byproduct is the spatial pattern of $M_{max}$ (Figure 7) over the study area. Estimated values range within the 6.0-8.5 interval, with higher values corresponding to a large sector of the south Aegean region. Our estimations are larger than those reported in the European Database of Seismogenic Faults (EDSF; http://diss.rm.ingv.it/share-edsf), where estimations have been done by taking into account the classic "magnitude - fault length" law-scale (e.g. Wells and Coppersmith, 1994). For most of the study area, differences in $M_{max}$ estimates are of ~0.4 on average, while differences up to 2 units of magnitude are observed along the Hellenic subduction zone. Such a relevant discrepancy would be related to the fact that estimation in the EDSF database has been performed by considering only crustal faults, while no estimates were included for the subduction interface. Moreover, our estimated values agree well with the ones reported in Bohnhoff et al. (2016) and Schäfer and Wenzel (2019) for NAFZ and the Hellenic subduction zone, respectively. Bohnhoff et al. (2016) compiled a catalog of events that occurred in the last 2300 years, and observed that the maximum earthquake magnitude increases with fault age, passing from values of ~7.4 along the western part up to ~8 on the eastern sector. Schäfer and Wenzel (2019) provided estimation of maximum magnitudes and associated return periods for 76 subduction zone segments by collecting various geologic, geodetic and seismological parameters and by using a machine learning classification along with other statistical methods. Regarding the entire Hellenic subduction zone, the same authors estimated a maximum magnitude of 8.6 with a return period of 514 years. Overall, although our estimations come from purely seismicity-based approaches (Kijko and Singh, 2011), results provide a realistic picture of the upper magnitude limits of large earthquakes that can strike the investigated region.

*6.2 Seismic coupling*

Geodetic moment-rates are a measure of elastic and anelastic loading rates, while the seismic moment-rates represent the elastic unloading rate. Their ratio (expressed as a percentage), is commonly termed as 'seismic coupling coefficient' (hereinafter SCC, Palano et al., 2018). Low SCC values indicate apparent seismic moment deficits where deformation could be either aseismically released across creeping faults and/or other crustal anelastic processes or accumulating for impending earthquakes (i.e. elastic storage). SCC values close to 100% indicate that the total deformation rate budget is released by crustal seismicity. In such cases, large earthquakes are the common behavior of faulting and the time-span after the past large event become an important indication of how temporally close the next could be. Observed outcomes usually fall into these two main categories, but cases with seismic moment-rates larger than the geodetic ones (SCC exceed 100%) are also possible (Pancha et al., 2006; Mazzotti et al., 2011).

SCC estimation for the Aegean-Anatolian area is reported in Figure 9b. Most of the area is characterized by low (< 35%) and intermediate (35% - 70% interval) SCC values, while only a few cells show values larger than 70% (with some cells exceeding 100%). Cells with high SCC values are located along a N-S-oriented boundary between western and central Anatolia, in the southeastern Peloponnese, along the eastern sector of the Hellenic volcanic arc, and at the NAZF and EAZF junction (Karliova triple junction); active faults in these regions are therefore fully coupled. Cells with intermediate SCC values are located in northern Albania, western Greece (CTF, Peloponnese and Gulf of Corinth), along the western sector of the Hellenic volcanic arc, southwestern of Crete, and western and south-eastern Turkey, suggesting an intermediate coupling for major tectonic elements, such as

EAFZ, western NAFZ (i.e. the fault segment close to Izmut area) and CTF and most of southern PSSZ. Low SCC values have been estimated for most of central and eastern Turkey, the offshore surrounding Cyprus, northern and central Greece and along most of the Hellenic subduction zone, pointing toward an aseismic behavior of active faults. Achieved results for the Aegean region generally agree with most of the previous findings (Ward, 1998; Jackson and McKenzie, 1988; Vernant et al., 2014; Jenny et al., 2004; Rontogianni, 2010; Chousianitis et al., 2015). Regarding Anatolia, our SCC estimates differ from the one performed by Ward (1998), pointing to a higher degree of coupling, especially on the western and central sectors of the region.

*6.2.1 General uncertainties and limits*

Several factors related to the deficiency in available geodetic (short time span, velocity uncertainties, density of stations, long-term deformation transient, etc.) and seismic (completeness and temporal length of catalogs, magnitude distribution and uncertainties, seismic cycle, etc.) data may affect the moment-rates estimation (see Palano et al., 2018 for additional details). Regarding the geodetic data, station density is (~$5 \times 10^{-4}$ site km$^2$ and ~$12.3 \times 10^{-4}$ site km$^2$ for Turkey and north-western Greece, respectively) close to the average value of western and central Europe (Masson et al., 2019; Sparacino et al., 2020). However, station density is ~$0.7 \times 10^{-5}$ site km$^2$ for the Aegean Sea, being affected by the spatial distribution of emerged islands. Besides such a low density, a minimum of 5 stations spatially well-distributed is always guaranteed for each computational grid, therefore providing robust strain-rate estimations. Our spatial density comes from a novel computation integrated with literature data that inevitably span different time periods. Few stations with a time interval of ~3 years (Tatar et al., 2012) sample the eastern part of the NAFZ, however the estimated GNSS velocities are in agreement with the ones coming from extensive InSAR datasets (Weiss et al., 2020). Aseismic postseismic deformation could affect velocity estimations on GNSS stations located in a region of 10-20 km from active faults, as observed for instance after the M7.4 1999 Izmit earthquake (e.g. Wang et al., 2009; Kaduri et al., 2017). Postseismic contribution is commonly removed during velocity estimation from continuous GNSS stations, while no corrections can readily be performed on episodic sites, therefore an unmodelled residual postseismic deformation could affect the few episodic stations close to the 1999 Izmit earthquake. However, this small segment of NAFZ is characterized by intermediate values, suggesting a moderate aseismic deformation. In addition, other few moderate earthquakes (M>5.5) occurred in the period covered by GNSS data, but no significant post-seismic effects have been detected on nearby sites.

Other major factors influencing the geodetic moment-rate estimations are the seismogenic thickness and the crustal rigidity modulus. We tested sensitivity to different values for these parameters. Following past approaches (Jenny et al., 2004; Ward, 1988; Rontogianni, 2010; Chousianitis et al., 2015), we performed a new estimation of the geodetic moment-rates, and consequently of the SCC, by assuming a uniform value of 15 km for the seismogenic thickness (see Figure S9a in Supplementary material). The resulting SCC values are not significantly different for the Anatolian region, while differences are observed for the Aegean region with a general increase of the SCC values, resulting in an increase of the number of cells with intermediate values at the expense of those with lower values. Another interesting difference is observed on CTF with SCC values, passing from intermediate to high ranges, in agreement with results reported in Chousianitis et al. (2015). Since Laigle et al. (2002) suggested that for a full seismic coupling on the Hellenic subduction zone, a shear modulus ranging from $1 \cdot 10^{10}$ N m$^{-2}$ to $2 \cdot 10^{10}$ N m$^{-2}$ is required, we performed an additional test, assuming a shear modulus of $2 \cdot 10^{10}$ N m$^{-2}$ (see Figure S9b in Supplementary material). The results again show an increase of the SCC values (with an obvious increasing number of cells with intermediate values at the expense of the ones with lower values) without however drastically changing the general pattern of SCC over the whole region. Geodetic moment-rate estimations can be influenced also by the

orientations of active faults within the investigated crustal volume (Carafa et al., 2017). This imply an increase of 15% of the moment-rate estimations for the regions where the dominant faulting style is normal or reverse, which on turn led to a decrease of the estimated SCC values. According to Carafa et al. (2017), we rescaled our geodetic moment-rate estimations by using the value of 2.31 instead of 2 in (eq. 5); results show a decrease of the SCC values without however changing the general pattern. All these tests highlighted that the assumptions of different parameters led to different geodetic moment-rate estimations. The range of all these estimations is narrow and the pattern of SCC over the whole region is not particularly influenced (see Figure S9 in Supplementary material). Our preferred moment-rates estimation (Figure 8c) falls within the above mentioned range, and can be considered as a realistic estimation for the whole study area.

Concerning the seismic data, both the duration and completeness of the seismic catalog govern their adequacy to estimate seismic moment-rates over a given region (e.g. Ward, 1998). A seismic catalog with a short duration (~100-300 years) could be insufficient to capture the seismic cycle of a given region. To acquire valid seismic moment-rates from seismic catalogs, the average earthquake recurrence interval should be shorter than the catalog duration (see Ward, 1988; Pancha et al., 2006; Mazzotti et al., 2011; Palano et al., 2018). Regarding our study area, the M5E catalog spans an average duration of ~770 years (Figure 9a) with ~90% of the computational cells above a duration greater than 400 years. As previously highlighted in paragraph 5.4, a duration of 400 years can be considered the minimal temporal length to reasonably capture the statistical long-term behavior of seismicity over the study area. Therefore, we conclude that the estimated seismic moment-rates (Figure 8a,b) are reliable for most of the study area. Regions with catalog duration shorter than 400 years concentrated on a large sector of north-central Turkey appear puzzling since they were characterized by large seismic events only in 1943 and 1994 (Figure 2 and Table S1 in Supplementary material). Furthermore, another two strong earthquakes, which occurred in 180 AD and 967 AD, are reported in Bohnhoff et al. (2016), suggesting long recurrence time or catalog incompleteness along this portion of NAFZ.

*6.3 Implications for seismic hazard*

The catalog incompleteness can be analyzed from the perspective of "missing earthquakes", i.e., the number of earthquakes of a given magnitude yearly necessary to match the difference between the geodetic and the seismic moment-rates (Mazzotti et al., 2011). For simplicity, in Figure 9c we considered the number of missing M7 earthquakes every 400 years for each 0.5° x 0.5° cell, as 1/16 of the amount of missing M7 earthquakes for each 2° x 2° cell. Although such a computation represents a gross estimation of missing earthquakes, it allows us to make some interesting considerations that can help better understand the SCC pattern over the study region. We can define at least four different groups. A first one, in central Turkey, is defined by cells with 0.1 to 1 M7 missing earthquakes. A second group, including north-western Greece, the Hellenic volcanic arc, and most of central and eastern Turkey along with some segments of both NAFZ and EAFZ, is characterized by cells with 1-3 missing earthquakes. A third group including the CTF, the northern and central Aegean Sea, northwestern Turkey and the offshore around Cyprus, is characterized by cells with 3-6 missing earthquakes, while the last group (cells with 6-12 missing earthquakes) includes the Hellenic subduction zone, a large region across the gulfs of Patras and Corinth, and a large sector across central and eastern NAFZ. Overall, such a computation reveals an unrealistic scenario of ~2400 M7 missing earthquakes, over a time interval of 400 years. Although both instrumental and historical seismic catalogs represent a random sampling of the long-term seismicity pattern over the whole seismic cycle of a given region, it is highly unrealistic to associate the observed moment-rate discrepancy only to the "missing earthquake" in the catalog. Assuming that 0.1 to 1 M7 missing earthquakes, over the 400 years, represent a realistic measure of the degree of catalog incompleteness, cells falling in the last three groups must be carefully considered.

Regarding the central and eastern segments of NAFZ, the "SCC-missing earthquake" patterns, as well as the spatial and temporal distributions of the past large earthquakes (Figure 9c), raise the possibility of impending earthquakes, especially for the sector comprised in the 35°-38° longitude range, characterized by few M≥7 earthquakes in the last 800 years (Figure 9a) with respect to the one occurring in the previous millennium (Bohnhoff et al., 2016). Similar considerations can be made for EAFZ, where however large earthquakes with M≥7 occurred only in the last 200 years despite the catalog duration of 800-900 years. Surface aseismic creeping has also been suggested for some local segments of EAFZ (Senturk et al., 2015). Moreover, the occurrence of several moderate-to-large earthquakes in historical time (Figure 2) points to a possible seismic gap along the fault system. All these aspects for EAFZ and eastern NAFZ are also supported by the low heat flux values (~60-70 $mW/m^2$; Artemieva and Shulgin, 2019), which indicate a crust with a normal thermal state.

The western segment of NAFZ is characterized by low to moderate SCC values, with highest values found near at local asperities detected by magnetotelluric data (Kaja et al., 2009) which also represents the focus of most historical and instrumental M≥7 earthquakes. The fracturing zone of NAFZ correlates well with crustal $V_P$ low-velocity (Koulakov et al., 2010), which coupled with the inferred SCC highlight a moderate aseismic component of deformation. Westward, along the north Aegean Trough, a considerable amount of the deformation mismatch is likely to occur aseismically, given the regional high heat flux values (>120 $mW/m^2$; e.g. Chamorro et al., 2014). Moreover, the possibility of a future M7 earthquake cannot be excluded given this region is the site of frequent large earthquakes (Figure 2).

Conversely, the central Aegean Sea can be considered a region with aseismic deformation because of the lack of large earthquakes in the last two millennia (Papazachos et al., 2010; Stucchi et al., 2013) and the occurrence of very few M6 earthquakes in the instrumental era (Figure 2). The deformation mismatch around the gulfs of Patras and Corinth requires numerous M7 earthquakes to be matched, while only few M>7 earthquakes are reported in historical catalogs (Papazachos et al., 2010; Stucchi et al., 2013). Since the seismic release of this region occurs predominantly through numerous M>6 earthquakes, as clearly documented for the last few centuries, the historical catalogs could be complete for such a magnitude only for the last two centuries, therefore a percentage of the observed deformation mismatch could be related to the catalog incompleteness, while the remaining part occurs in aseismic mode.

Among these regions, the Hellenic subduction zone is the most interesting since it has experienced two M>8 earthquakes in the last two millennia, in 365 CE (Papazachos et al., 2010) and 1303 CE (Papazachos et al., 2010; Stucchi et al., 2013), respectively. Our gross estimation of missing earthquakes indicates that ~1400 M7 earthquakes are required to fill the deformation mismatch. Such an estimation is unrealistic, and suggests that a part of the deformation is aseismic within the Hellenic subduction (Apel, 2011), or that future M8+ earthquakes are possible. Subduction complexes generally consist of metamorphosed rocks, together with clastic and pelagic sediments, which form a zone up to several kilometers thick to depths of at least 40 km. At temperatures above ~ 350 °C (corresponding to > 25-35 km depth), the subduction zone undergoes a transition to aseismic behavior, and much of the relative motion between converging plates occurs as ductile deformation (e.g. Platt et al., 2018). Moreover, as above mentioned, a future M8 earthquake cannot be ruled out, because of the high convergence rate and the lack of large magnitude earthquakes in the last 700 years.

Finally, our results are generally consistent with the more recent seismic hazard models available for the region (e.g. Woessner et al., 2015). The growth of continuous GNSS networks in the last decade allowed the acquisition of continuous and spatially extensive datasets over large regions of the Earth. The high resolution geodetic strain-rate can be considered as an additional data type to constrain further the probability of occurrence and the magnitude of future earthquakes. Recent hazard models of long-term probabilistic seismic hazard analysis (e.g. Gerstenberger et al. 2020; Visini et al.,

2021; Stevens and Avouac, 2021) consider geodetic data. We anticipate that as non-seismological workflows describe ground deformation with increasing robustness (e.g. Rouet-Ledouc et al., 2021), the inclusion of different data types in short- and long-term hazard models will improve current approaches.

### *6. Conclusive remarks*

We reviewed kinematics and tectonics for the Aegean-Anatolian region to acquire an improved estimation of the seismic coupling by merging and analyzing extensive seismic and geodetic datasets. To quantify the seismic coupling, we estimate by-products, such as the seismogenic thickness, the expected maximum magnitude, *a*- and *b-value* of the frequency-magnitude earthquake distribution and the magnitude of completeness of the instrumental catalog, for the first time homogeneously over a complex plate margin as that in the eastern Mediterranean area. We find:

- Regions with nearly full seismic coupling, such as the region surrounding the Karliova triple junction, a N-S-oriented belt along the boundary between western and central Anatolia, and the southeastern Peloponnese. Regarding the Karliova triple junction, the short time period since the earthquake (~80 years) potentially precludes the occurrence with similar magnitude at least in the next century. Nonetheless, impending earthquakes with moderate magnitude cannot be ruled out given the high deformation rate of the region. Regarding the N-S-oriented belt, given the occurrence of only one large earthquake (the 1914 $M_w$ 7.1 Burder event), the observed deformation rate appears compensated by several moderate earthquakes, mainly concentrated along the active faults. Similar interpretations are perhaps valid for the southeastern Peloponnese.
- Regions with intermediate seismic coupling, such as the Eastern Anatolian fault zone, western and central segments of the Northern Anatolian fault zone, part of the Hellenic volcanic arc, the CTF and the active faults in the gulfs of Patras and Corinth. For these regions, the intermediate coupling could be partially attributed to the aseismic components of deformation and to catalog incompleteness. Moreover, the temporal distribution of the past large earthquakes also indicates a high possibility of impending earthquakes at the Eastern Anatolian fault zone, and along the western and central segments of the Northern Anatolian fault zone.
- Regions where aseismic deformation prevails, such as in the central Aegean Sea, with modest seismic release over the last millennium.
- Regions identified as potential seismic gaps (small coupling and absence of large earthquakes) such as parts of the Hellenic subduction zone.

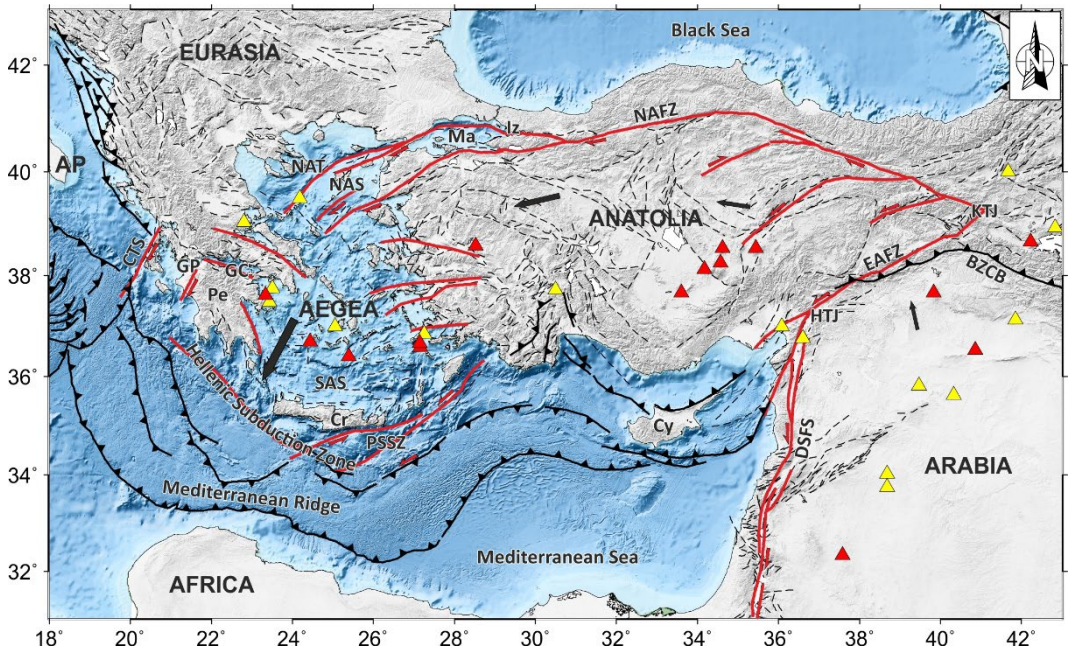


**Figure 1**. Tectonic setting of the Aegean-Anatolia region. Major faults and thrusts are reported in red and black, respectively, while minor tectonic lineaments are reported as dashed black lines (from the European Database of Seismogenic Faults; Palano et al., 2013). The black arrows represent the GNSS motion across the Anatolian and Aegean blocks. Holocene and Pleistocene volcanoes (https://volcano.si.edu) are reported as yellow and red triangles, respectively. Abbreviations are: Ma, Marmara Sea; NAT, North Aegean Trough; CTS, Cefalonia transform fault; GP, Gulf of Patras; GC, Gulf of Corinth; Pe, Peloponnese; NAS, North Aegean Sea; SAS, South Aegean Sea; Cr, Crete, PSSZ, Pliny-Strabo shear zone; Cy, Cyprus; NAFZ, North Anatolian fault zone, East Anatolian fault Zone; KTJ, Karliova triple junction; HTJ, Hatay triple junction; DSFS, Dead Sea fault system; BZCB, Bitlis-Zagros collisional belt; Ap, Apulia.

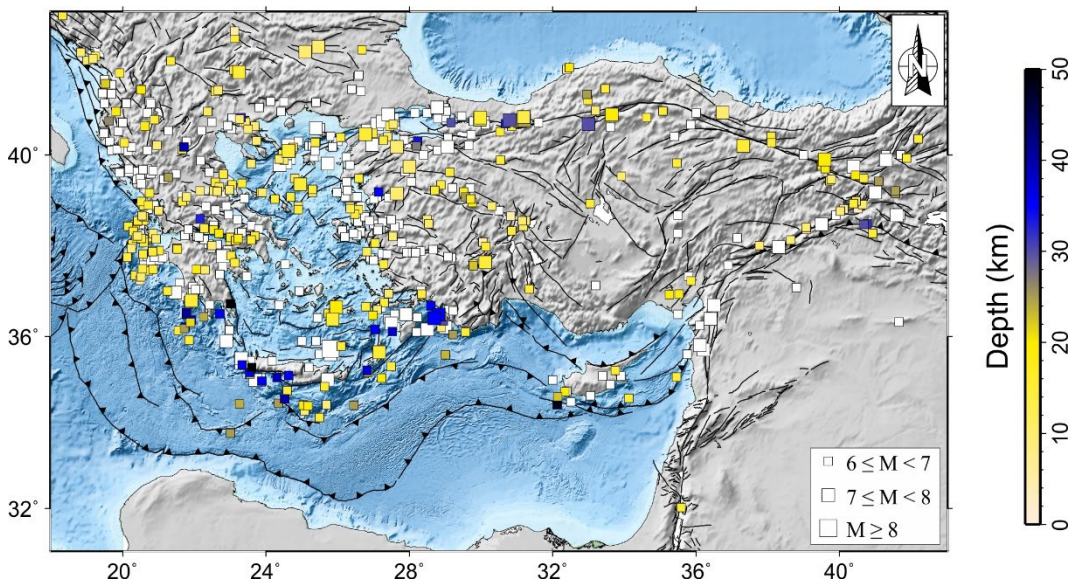


**Figure 2**. Strong historical (1003 - 1903) and instrumental (August 1903 - December 2020) earthquakes (M≥7) in the Aegean-Anatolian region.

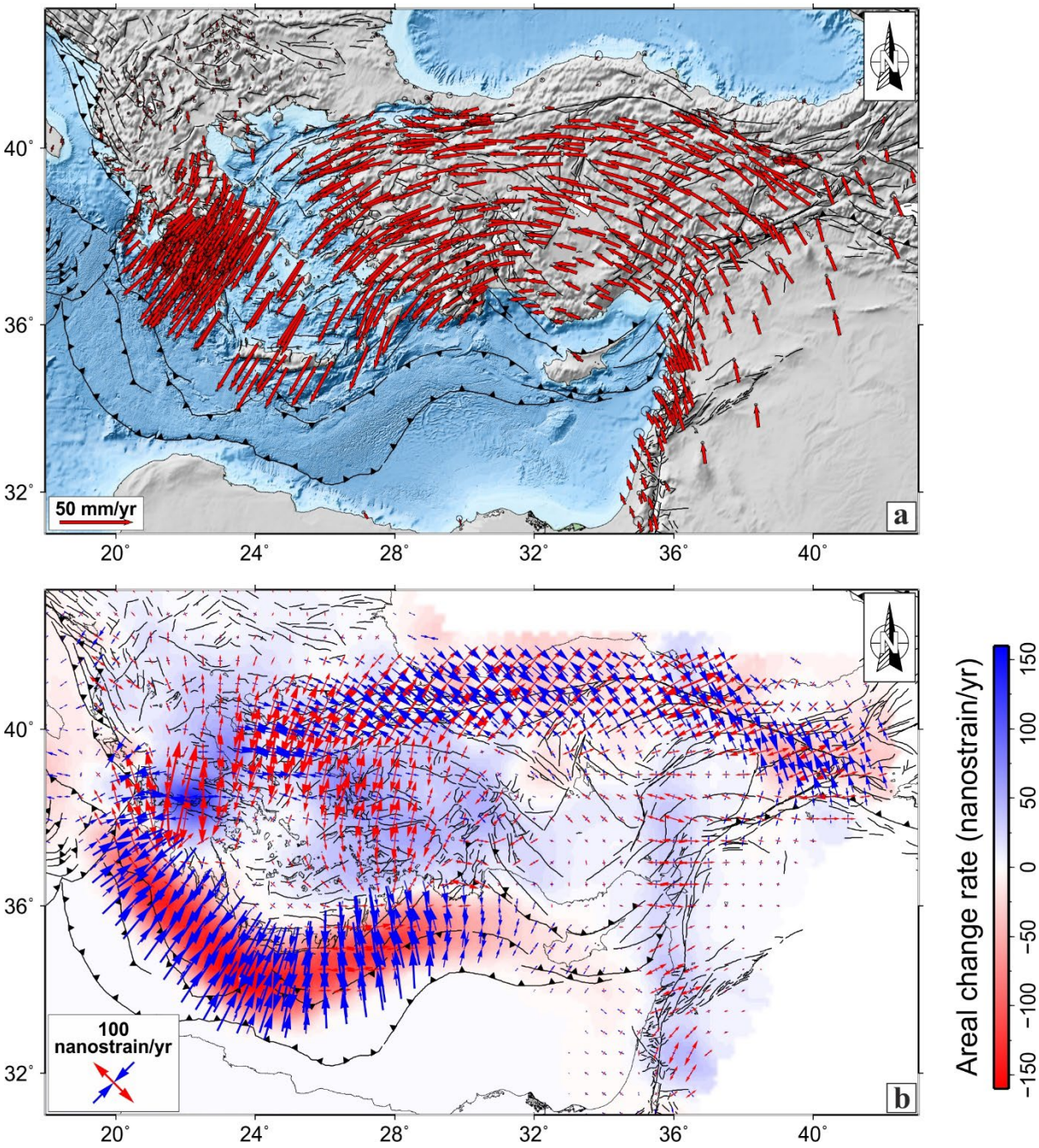


**Figure 3**. a) GNSS velocities and 95% confidence ellipses in a fixed Eurasian plate. b) Geodetic strain-rate field: the background color represents the rate of areal change, while arrows represent the greatest extensional (red) and contractional (blue) horizontal strain-rates.

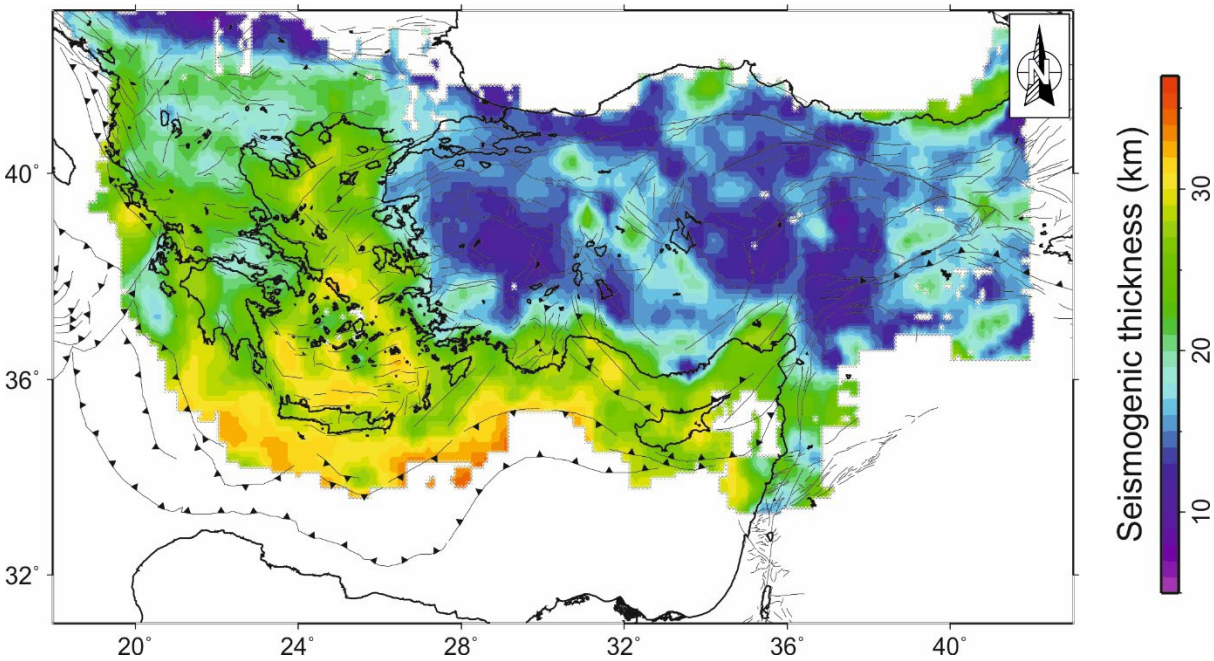


**Figure 4**. Seismogenic thickness pattern beneath the Aegean-Anatolian region. See also Figure S7 in the supplementary material for additional details.

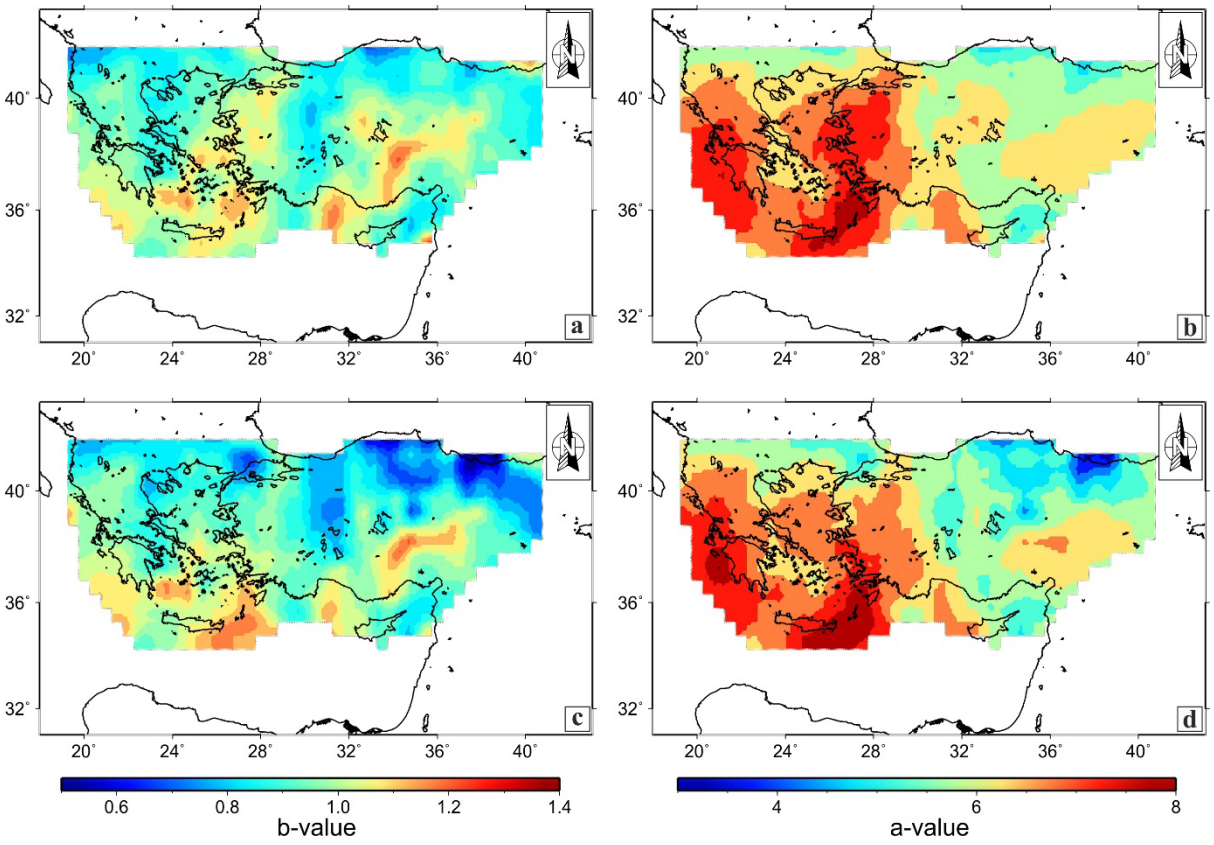


**Figure 5**. Spatial pattern of *a*- and *b-values* for the Aegean-Anatolian region as estimated by the MLE (panels a and b) and the RFM (panels c and d) approaches, respectively.

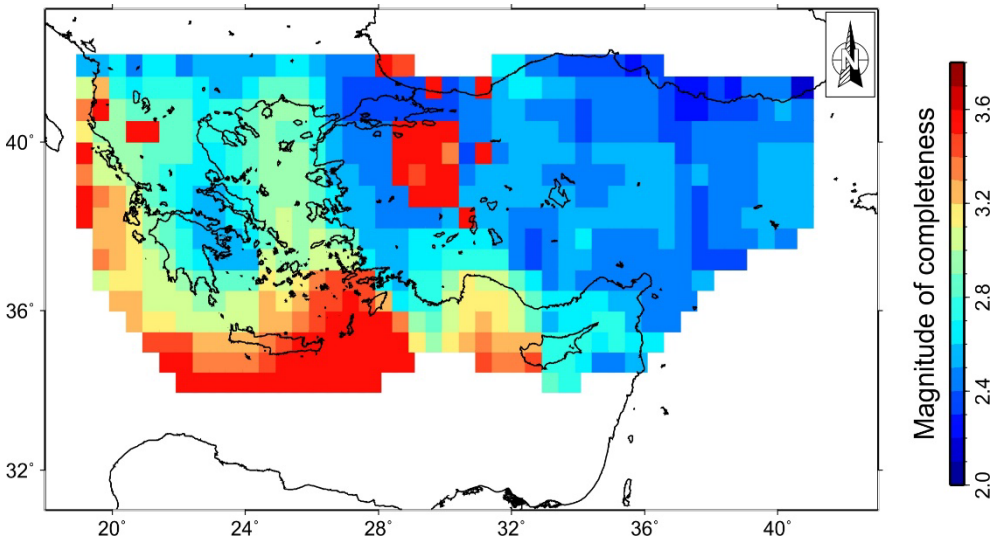


**Figure 6**. Spatial pattern of the magnitude of completeness (*Mc*).

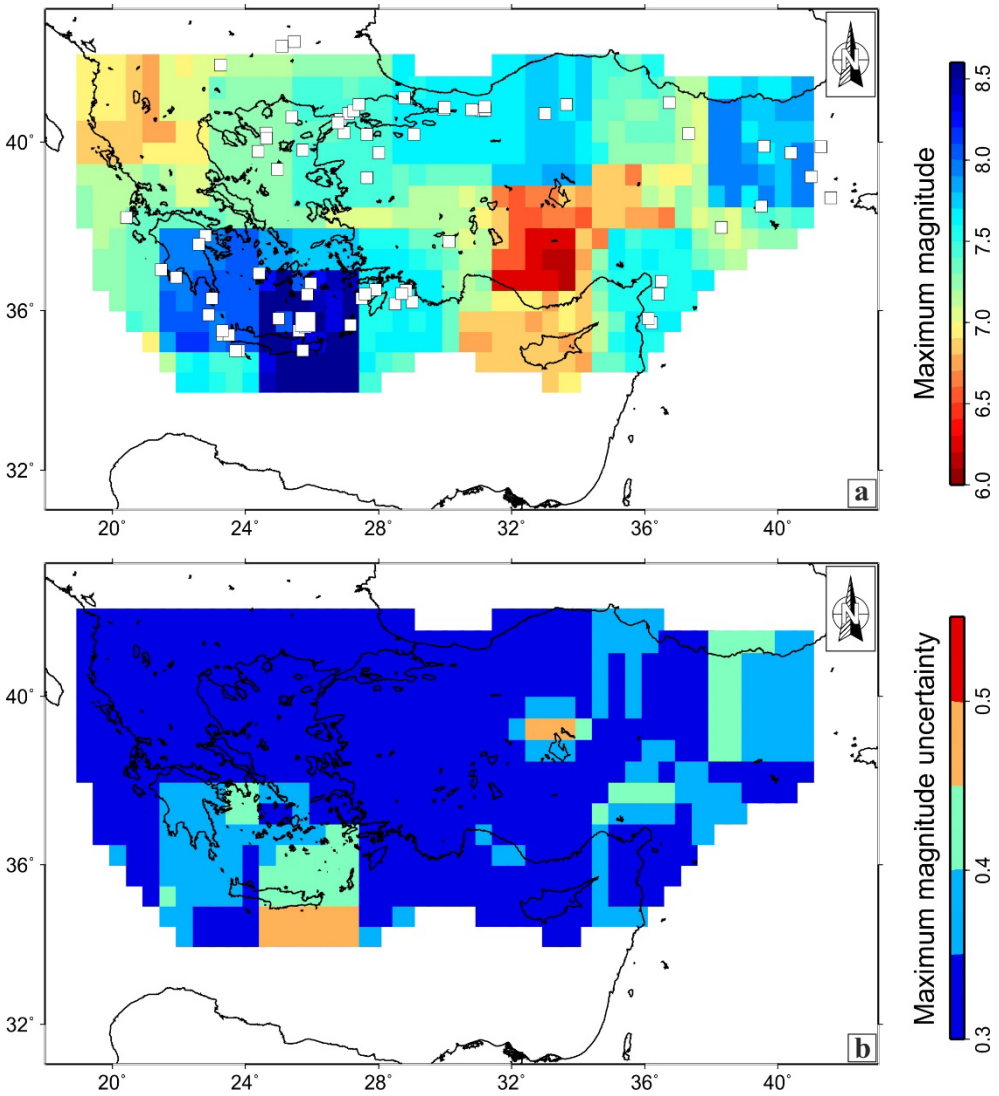


**Figure 7**. Spatial pattern of estimated maximum (a) along with its estimated uncertainties (b). Historical and instrumental large earthquakes (M≥7) are also reported.

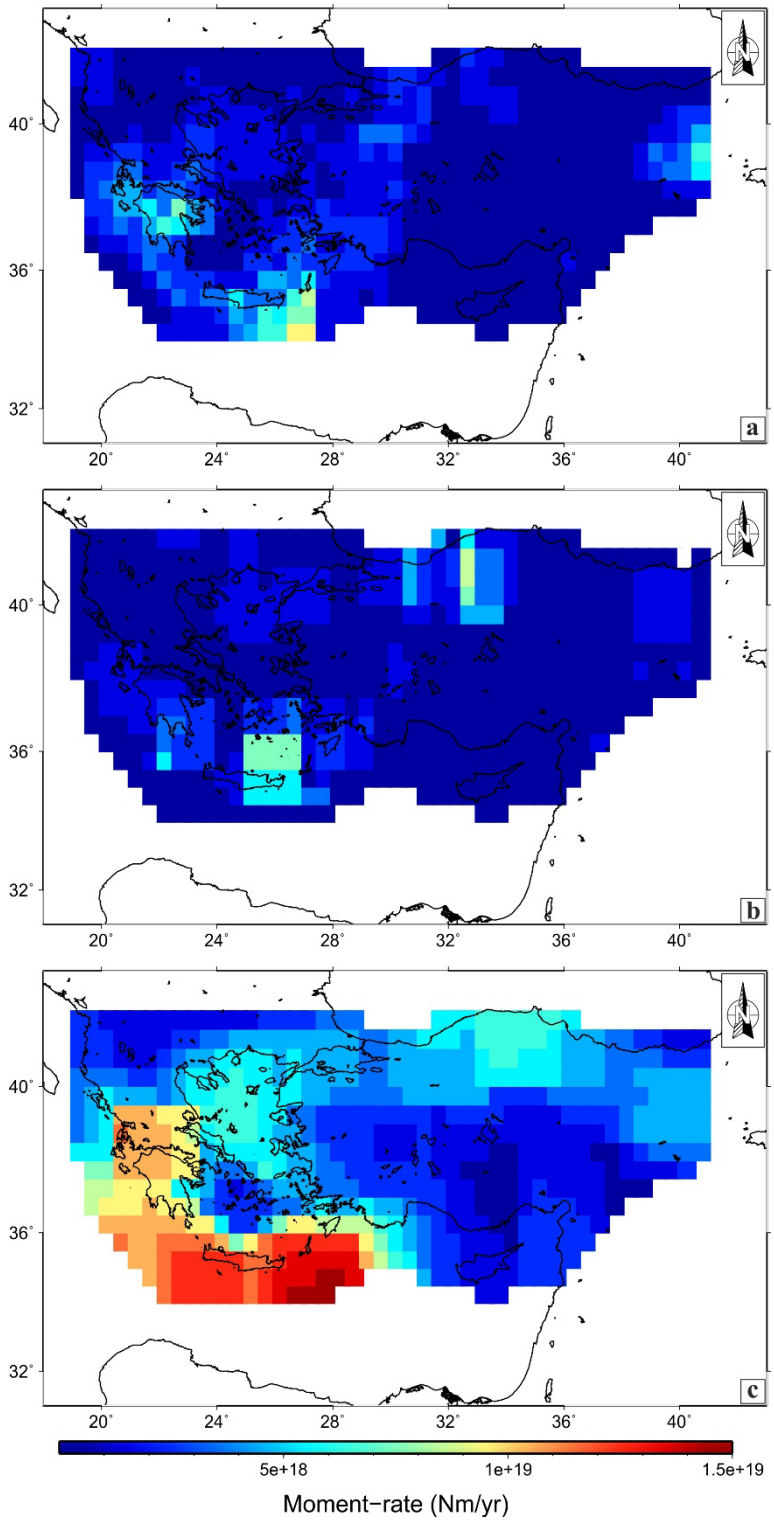


**Figure 8**. Estimated moment-rates from a) instrumental seismicity, by considering the truncated Gutenberg-Richter distribution (eq. 1), b) historical and instrumental seismicity, by considering the cumulative Kostrov summation method (eq. 4), and c) geodetic data (eq. 5). It should be noted that moment-rates are plotted on a 0.5° x 0.5° grid, while in fact they refer to the 2° x 2° computational grid.

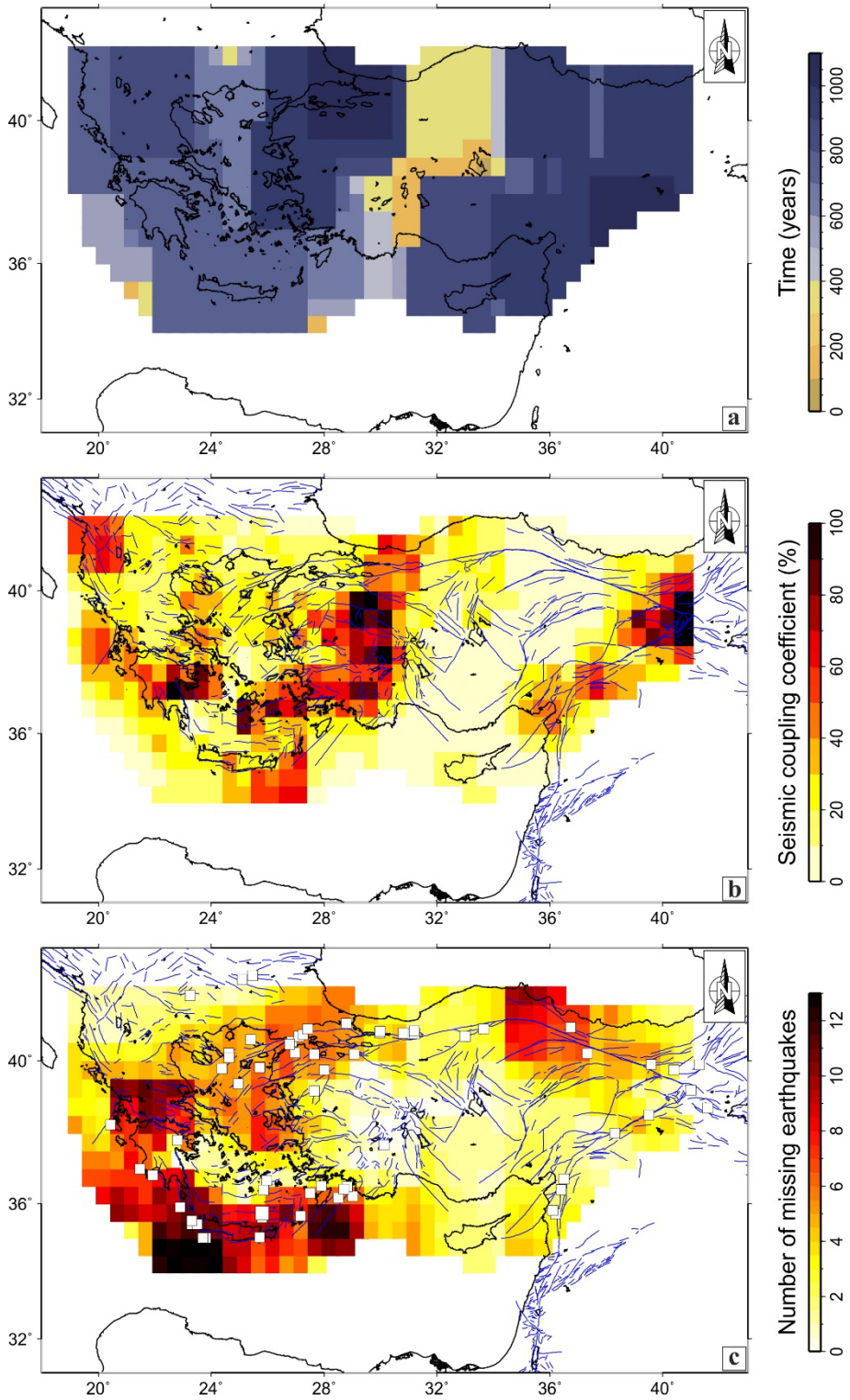


**Figure 9**. a) Spatial pattern of temporal duration of the M5C catalog. b) Spatial pattern of the seismic coefficient coupling (SCC). c) Missing earthquakes over a time interval of 400 years.

| Author | Moment-rates | | $H_S$ (km) | $\mu$ ($10^{10}$ N m$^{-2}$) | Results |
|---|---|---|---|---|---|
| | Seismic | Geologic/Geodetic | | | |
| Jackson and McKenzie, (1988) | M≥6 earthquake in the 1908-1981 interval and using [1] | Geological plate deformation rates adopting [1] | 10 | 3 | Aseismic deformation along the Hellenic trench (10%) and in eastern Turkey (10-40%). Seismic deformation (~100%) for Aegean, western Turkey and along the NAFZ. |
| Ward (1998) | Large earthquake in the 1900-1995 interval and using [1] | Geodetic velocity from VLBI, SLR and GPS observations; rates estimated adopting [1] | 10 (Anatolia) 15 (Aegean) | 3 | Aseismic deformation for Turkey (seismic coupling of 22%); moderate seismic coupling (62%) in the Aegean. |
| Laigle et al. (2002) | Moment-rates have been modelled using [2] | Moment-rates have been modelled using [2] | 50 | 3 | A full seismic coupling for the Hellenic subduction zone may be achieved only with low shear modulus (e.g. 1-2 · $10^{10}$ N m$^{-2}$. |
| Vernant et al. (2014) | Estimations coming from Jackson and McKenzie, (1988) | Geodetic velocities modelled with a block model approach; moment-rates estimated with [3] | 15 - 45 | 3 | Aseismic deformation (seismic coupling of 10%) along the Hellenic subduction interface. |
| Jenny et al. (2004) | Two seismic catalogs covering respectively the last 500 and 2550 years. Moment-rates estimated following [4]. | Geodetic velocity field compiled by literature and spanning the 1988 - 1997 period; moment-rates estimated adopting [5] | 15 | 3.5 | Full seismic coupling for CTF and western NAFZ; The Hellenic trench is largely uncoupled, with at least 50-90% of the total deformation released aseismically. At the remainder of the study, a 10-30% of the total deformation is aseismic. |
| Rontogianni (2010) | Earthquake catalogs with periods of 30, 100 and 300 years; strain-rates estimated following [1]. | Geodetic velocity field spanning the 1994-2000 period. | 15 | 3.5 | For the majority of Greek region, the geodetic strain-rates are larger than the seismic ones. The deficit will be released by future earthquake. |
| Chousianitis et al. (2015) | Seismic catalog covering the 1300-2014 period. Moments-rates estimated following [6] | Geodetic velocity field spanning the 2003-2013 period. Moment-rates estimated adopting [1] | 15 | 3 | Full seismic coupling for central Ionian Sea, while in other areas, the geodesy-based moment-rates were at least 2 times higher than the earthquake-based. |

**Table 1.** Summary of previous moment-rates estimation over the investigated region. [1] Kostrov, 1984; [2] Brune, 1968; [3] Aki, 2002; [4] Hyndman and Weichert (1983); [5] Savage and Simpson (1997); [6] Molnar (1979). Percentages reported in the column "Results" refer to the Seismic coupling coefficient as defined in this study.

**Acknowledgements.** We thank the Editor Gillian R. Foulger and two anonymous reviewers for constructive reviews of this paper. We acknowledge UNAVCO (www.unavco.org), EUREF (www.epncb.oma.be), SOPAC (http://sopac.ucsd.edu) and NGS (http://geodesy.noaa.gov) for providing free access to GNSS data. We also acknowledge NOA (http://www.gein.noa.gr/en/), KOERI (http://www.koeri.boun.edu.tr) and ISC for providing free access to seismic catalogs.

## References

Aki, K., 1966. Generation and propagation of G waves from the Niigata earthquake of June 14, 1964. Part 2. Estimation of earthquake moment, released energy and stress-strain drop from G wave spectrum. Bull. Earth. Res. Ins., *44, 73-88*.

Aktuğ, B., Parmaksız, E., Kurt, M., Lenk, O., Kılıçoğlu, A., Gürdal, M.A., Özdemir, S., 2013. Deformation of Central Anatolia: GPS implications. J. Geodyn. 67, 78-96. https://doi.org/10.1016/j.jog.2012.05.008.

Apel, E. W., 2011. Shells on a Sphere: Tectonic Plate Motion and Plate Boundary Deformation. PhD. Dissertation, University of California, Berkeley, USA, https://escholarship.org/uc/item/7xm5z7bb

Artemieva, I.M., Shulgin, A., 2019. Geodynamics of Anatolia: Lithosphere thermal structure and thickness. Tectonics 38(12), 4465-4487. https://doi.org/10.1029/2019TC005594.

Basili, R., Tiberti, M.M., Kastelic, V., Romano, F., Piatanesi, A., Selva, J., Lorito, S., 2013. Integrating geologic fault data into tsunami hazard studies. Nat. Hazards Earth Syst. Sci. 13(4), 1025-1050. https://doi.org/10.5194/nhess-13-1025-2013.

Bogazici University – Kandilli Observatory and Earthquake Research Institute – Regional Earthquake-Tsunami Monitoring Center. http://www.koeri.boun.edu.tr/sismo/2/earthquake-catalog (accessed on 19 July 2021).

Bohnhoff, M., Martínez-Garzón, P., Bulut, F., Stierle, E., Ben-Zion, Y., 2016. Maximum earthquake magnitudes along different sections of the North Anatolian fault zone. Tectonophysics 674, 147-165. https://doi.org/10.1016/j.tecto.2016.02.028.

Brune, J. N., 1968. Seismic moment, seismicity, and rate of slip along major fault zones. J. Geophys. Res., 73(2), 777-784. doi:10.1029/JB073i002p00777.

Bulut, F., Aktar, M., 2007. Accurate relocation of İzmit earthquake (Mw = 7.4, 1999) aftershocks in Çınarcık Basin using double difference method. Geophys. Res. Lett. 34, L10307. https://doi.org/10.1029/2007GL029611.

Bulut, F., Bohnhoff, M., Eken, T., Janssen, C., Kılıç, T., Dresen, G., 2012. The East Anatolian Fault Zone: Seismotectonic setting and spatiotemporal characteristics of seismicity based on precise earthquake locations. J. Geophys. Res.: Solid Earth 117(B7). https://doi.org/10.1029/2011JB008966.

Carafa, M.M.C., Valensise, G., Bird, P., 2017. Assessing the seismic coupling of shallow continental faults and its impact on seismic hazard estimates: a case-study from Italy. Geophys. J. Int. 209, 32-47. https://doi.org/10.1093/gji/ggx002.Chamorro, C.R., García-Cuesta, J.L., Mondéjar, M.E., Pérez-Madrazo, A., 2014. Enhanced geothermal systems in Europe: An estimation and comparison of the technical and sustainable potentials. Energy 65, 250-263. https://doi.org/10.1016/j.energy.2013.11.078.

Chiarabba, C., De Gori, P., 2016. The seismogenic thickness in Italy: constraints on potential magnitude and seismic hazard. Terra Nova 28(6), 402-408. https://doi.org/10.1111/ter.12233.

Chousianitis, K., Ganas, A., Evangelidis, C.P., 2015. Strain and rotation rate patterns of mainland Greece from continuous GPS data and comparison between seismic and geodetic moment release. J. Geophys. Res. 120, 3909–3931. https://doi.org/10.1002/2014JB011762.

Corbi, F., Herrendörfer, R., Funiciello, F., Van Dinther, Y., 2017. Controls of seismogenic zone width and subduction velocity on interplate seismicity: Insights from analog and numerical models. Geophys. Res. Lett. 44(12), 6082-6091. https://doi.org/10.1002/2016GL072415.

D'Agostino, N., 2014. Complete seismic release of tectonic strain and earthquake recurrence in the Apennines (Italy). Geophys. Res. Lett. 41(4), 1155-1162. https://doi.org/10.1002/2014GL059230.

D'Agostino, N., Métois, M., Koci, R., Duni, L., Kuka, N., Ganas, A., Georgiev, I., Jouanne, F., Kaludjerovic, N., Kandić, R., 2020. Active crustal deformation and rotations in the southwestern Balkans from continuous GPS measurements. Earth Planet. Sci. Lett. 539, 116246. https://doi.org/10.1016/j.epsl.2020.116246.

Déprez, A., Doubre, C., Masson, F., Ulrich, P., 2013. Seismic and aseismic deformation along the East African Rift System from a reanalysis of the GPS velocity field of Africa. Geophys. J. Int. 193, 1353–1369. https://doi:10.1093/gji/ggt085.

Doutsos, T., Koukouvelas, I. K., Xypolias, P., 2006. A new orogenic model for the External Hellenides. Geol. Soc., London, Special Publication 260, 507-520. https://doi.org/10.1144/GSL.SP.2006.260.01.21.

England, P., Houseman, G., Nocquet, J.M., 2016. Constraints from GPS measurements on the dynamics of deformation in Anatolia and the Aegean. J. Geophys. Res.: Solid Earth 121(12), 8888-8916. https://doi.org/10.1002/2016JB013382

Erdik, M., Biro, Y.A., Onur, T., Sesetyan, K., Birgoren, G., 1999. Assessment of earthquake hazard in Turkey and neighboring. Annals of Geophysics 42(6). https://doi.org/10.4401/ag-3773.

Frohlich, C., Davis, S.D., 1993. Teleseismic b values; or, much ado about 1.0. J. Geophys. Res.: Solid Earth 98(B1), 631-644. https://doi.org/10.1029/92JB01891.

Ganas, A., Parsons, T., 2009. Three-dimensional model of Hellenic Arc deformation and origin of the Cretan uplift. J. Geophys. Res.: Solid Earth 114(B6). https://doi.org/10.1029/2008JB005599.

Giardini, D., et al., 2013. Seismic Hazard Harmonization in Europe (SHARE): Online Data Resource. https://doi:10.12686/SED-00000001-SHARE.

Giardini, D., Wössner, J., Danciu, L., 2014. Mapping Europe's seismic hazard. Eos, Transactions American Geophysical Union 95(29), 261-262. https://doi.org/10.1002/2014EO290001.

Global Volcanism Program, Smithsonian Institution *National Museum of Natural History*. https://volcano.si.edu (accessed 19 July 2021).

Grosser, H., Baumbach, M., Berckhemer, H., Baier, B., Karahan, A., Schelle, H., Kruger, F., Paulat, A., Michel, G., Demirtas, R., Gencoglu, S., Yilmaz, R., 1998. The Erzincan (Turkey) earthquake (Ms 6.8) of March 13, 1992 and its aftershock sequence. Pure Appl. Geophys. 152(3), 465-505. https://doi.org/10.1007/s000240050163.

Grünthal, G., Wahlström, R., Stromeyer, D., 2013. The SHARE European Earthquake Catalogue (SHEEC) for the time period 1900-2006 and its comparison to the European-Mediterranean Earthquake Catalogue (EMEC). J. Seismolog. 17(4), 1339-1344. https://doi.org/10.1007/s10950-013-9379-y.

Gerstenberger, M. C., Marzocchi, W., Allen, T., Pagani, M., Adams, J., Danciu, L., Field E. H., Fujiwara, H., Luco, N., Ma, K.-F., Petersen, M. D., 2020. Probabilistic seismic hazard analysis at regional and national scales: State of the art and future challenges. Rev. Geophys. 58(2), e2019RG000653. https://doi.org/10.1029/2019RG000653.

Gutenberg, B., Richter, C.F., 1956. Earthquake magnitude, intensity, energy, and acceleration: (Second paper). Bull. Seismol. Soc. Am. 46(2), 105-145. https://doi.org/10.1785/BSSA0460020105.

Han, Q., Wang, L., Xu, J., Carpinteri, A., Lacidogna, G., 2015. A robust method to estimate the b-value of the magnitude–frequency distribution of earthquakes. Chaos, Solitons Fractals 81, 103-110. https://doi.org/10.1016/j.chaos.2015.09.004.

Hanks, T.C., Kanamori, H., 1979. A moment magnitude scale. J. Geophys. Res. 84, 2348–2350. https://doi:10.1029/JB084iB05p02348.

Herring, T.A., King, R.W., Floyd, M.A., McClusky, S.C., 2018. Introduction to GAMIT/GLOBK, Release 10.7; Massachusetts Institute of Technology: Cambridge, UK.

Howell, A., Jackson, J., Copley, A., McKenzie, D., Nissen, E., 2017. Subduction and vertical coastal motions in the eastern Mediterranean. Geophys. J. Int. 211(1), 593-620. https://doi.org/10.1093/gji/ggx307.

Hyndman, R.D., Weichert, D.H., 1983. Seismicity and rates of relative plate motion on the plate boundaries of western North America. Geophys. J. R. Astron. Soc. 72, 59–82. https://doi:10.1111/j.1365-246X.1983.tb02804.x.

Institute of Geodynamics – National Observatory of Athens. http://www.gein.noa.gr/en/seismicity/earthquake-catalogs (accessed on 19 July 2021).

International Seismological Centre (20XX), ISC-GEM Earthquake Catalogue. http://www.isc.ac.uk/iscgem/index.php (accessed on 19 July 2021).

International Seismological Centre. http://www.isc.ac.uk/ (accessed on 19 July 2021).

Jackson, J., McKenzie, D., 1988. The relationship between plate motions and seismic moment tensors, and the rates of active deformation in the Mediterranean and Middle East. Geophys. J. Int. 93(1), 45-73. https://doi.org/10.1111/j.1365-246X.1988.tb01387.x.

Jenny, S., Goes, S., Giardini, D., Kahle, H.G., 2004. Earthquake recurrence parameters from seismic and geodetic strain rates in the eastern Mediterranean. Geophys. J. Int. 157(3), 1331-1347. https://doi.org/10.1111/j.1365-246X.2004.02261.x.

Jolivet, L., Brun, J.P., 2010. Cenozoic geodynamic evolution of the Aegean. Int. J. Earth Sci. (Geol. Rundsch) 99 (1), 109-138. https://doi.org/10.1007/s00531-008-0366-4.

Jolivet, L., Faccenna, C., 2000. Mediterranean extension and the Africa-Eurasia collision. Tectonics 19(6), 1095-1106. https://doi.org/10.1029/2000TC900018.

Jolivet, L., Faccenna, C., Huet, B., Labrousse, L., Le Pourhiet, L., Lacombe, O., Lecomte, E., Burov, E., Denèle, Y., Brun, J., Philippon, M., Paul, A., Salaün, G., Karabulut, H., Piromallo, C., Monié, P., Gueydan, F., Okay, A.I., Oberhänsli, R., Pourteau, A., Augier, R., Gadenne, L., Driussi, O., 2013. Aegean tectonics: Strain localisation, slab tearing and trench retreat. Tectonophysics 597, 1-33. https://doi.org/10.1016/j.tecto.2012.06.011.

Kaduri, M., Gratier, J.P., Renard, F., Çakir, Z., Lasserre, C., 2017. The implications of fault zone transformation on aseismic creep: Example of the North Anatolian Fault, Turkey. J. Geophys. Res.: Solid Earth 122(6), 4208-4236. https://doi.org/10.1002/2016JB013803.

Kalyoncuoglu, U.Y., 2007. Evaluation of seismicity and seismic hazard parameters in Turkey and surrounding area using a new approach to the Gutenberg–Richter relation. J. Seismolog. 11(2), 131-148. https://doi.org/10.1007/s10950-006-9041-z.

Kaya, T., Tank, S.B., Tunçer, M.K., Rokoityansky, I.I., Tolak, E., Savchenko, T., 2009. Asperity along the North Anatolian Fault imaged by magnetotellurics at Düzce, Turkey. Earth Planets Space 61(7), 871-884. https://doi.org/10.1186/BF03353198.

Kijko, A., Graham, G., 1998. Parametric-historic procedure for probabilistic seismic hazard analysis Part I: estimation of maximum regional magnitude mmax. Pure Appl. Geophys. 152(3), 413–442. https://doi.org/10.1007/s000240050161.

Kijko, A., Singh, M., 2011. Statistical tools for maximum possible earthquake magnitude estimation. Acta Geophys. 59, 674-700. https://doi.org/10.2478/s11600-011-0012-6.

Kostrov, V., 1974. Seismic moment and energy of earthquakes, and seismic Row of rock. Izv. Acad. Sci. USSR Phys. Solid Earth 1, 23–44.

Koulakov, I., Bindi, D., Parolai, S., Grosser, H., Milkereit, C., 2010. Distribution of seismic velocities and attenuation in the crust beneath the North Anatolian Fault (Turkey) from local earthquake tomography. Bull. Seismol. Soc. Am. 100(1), 207-224. https://doi.org/10.1785/0120090105.

Kokkalas, S., Xypolias, P., Koukouvelas, I., Doutsos, T., 2006. Postcollisional contractional and extensional deformation in the Aegean region. Geol. Soc. Am., Special Paper 409, 97-123. https://doi.org/10.1130/0-8137-2409-0.97.

Koukouvelas, I. K., Aydin, A., 2002. Fault structure and related basins of the North Aegean Sea and its surroundings. Tectonics 21(5), 10-1. https://doi.org/10.1029/2001TC901037.Laigle, M., Hirn, A., Sachpazi, M., Clément, C., 2002. Seismic coupling and structure of the Hellenic subduction zone in the Ionian Islands region. Earth Planet. Sci. Lett. 200(3-4), 243-253. https://doi.org/10.1016/S0012-821X(02)00654-4.

Le Pichon, X., Kreemer, C., 2010. The Miocene-to-present kinematic evolution of the Eastern Mediterranean and Middle East and its implications for dynamics. Annu. Rev. Earth Planet. Sci. 38, 323-351. https://doi.org/10.1146/annurev-earth-040809-152419.

Louvari, E., Kiratzi, A.A., Papazachos, B.C., 1999. The Cephalonia transform fault and its extension to western Lefkada Island (Greece). Tectonophysics 308(1-2), 223-236. https://doi.org/10.1016/S0040-1951(99)00078-5.

Mahmoud, Y., Masson, F., Meghraoui, M., Cakir, Z., Alchalbi, A., Yavasoglu, H., Yönlü, O., Daoud, M., Ergintav, S., Inan, S., 2013. Kinematic study at the junction of the East Anatolian fault and the Dead Sea fault from GPS measurements. J. Geodyn. 67, 30-39. https://doi.org/10.1016/j.jog.2012.05.006.

Masson, F., Chéry, J., Hatzfeld, D., Martinod, J., Vernant, P., Tavakoli, F., Ghafory-Ashtiani, M., 2005. Seismic versus aseismic deformation in Iran inferred from earthquakes and geodetic data. Geophys. J. Int. 160, 217–226. https://doi:10.1111/j.1365-246X.2004.02465.x.

Masson, C., Mazzotti, S., Vernant, P., Doerflinger, E., 2019. Extracting small deformation beyond individual station precision from dense Global Navigation Satellite System (GNSS) networks in France and western Europe. Solid Earth, 10(6), 1905-1920. https://doi.org/10.5194/se-10-1905-2019.

Mazzotti, S., Leonard, L.J., Cassidy, J.F., Rogers, G.C., Halchuk, S., 2011. Seismic hazard in western Canada from GPS strain rates versus earthquake catalog. J. Geophys. Res. 116, B12310. https://doi:10.1029/2011JB008213.

McKenzie, D.P., Davies, D., Molnar, P., 1970. Plate tectonics of the Red Sea and east Africa. Nature 226(5242), 243-248. https://doi.org/10.1038/226243a0.

McNutt, S.R., 2005. Volcanic seismology. Annu. Rev. Earth Planet. Sci. 32, 461-491. https://doi.org/10.1146/annurev.earth.33.092203.122459.

Métois, M., D'Agostino, N., Avallone, A., Chamot-Rooke, N., Rabaute, A., Duni, L., Kuka, N., Koci, R., Georgiev, I., 2015. Insights on continental collisional processes from GPS data: Dynamics of the peri-Adriatic belts. J. Geophys. Res.: Solid Earth 120(12), 8701-8719. https://doi.org/10.1002/2015JB012023.

Métois, M., Socquet, A., Vigny, C., Carrizo, D., Peyrat, S., Delorme, A., Maureira, E., Valderas-Bermejo, M.-C., Ortega, I., 2013. Revisiting the North Chile seismic gap segmentation using GPS-derived interseismic coupling. Geophys. J. Int. 194(3), 1283-1294. https://doi.org/10.1093/gji/ggt183.

Miller, C.K., Furlong, K.P., 1988. Thermal-mechanical controls on seismicity depth distributions in the San Andreas Fault Zone. Geophys. Res. Lett. 15(12), 1429-1432. https://doi.org/10.1029/GL015i012p01429.

Mogi, K., 1962. Study shocks caused by the fracture of heterogeneous materials and its relations to earthquake phenomena. Bulletin of Earthquake Research Institute, University of Tokyo 40, 123-173.

Molnar, P., 1979. Earthquake recurrence intervals and plate tectonics. Bull. Seism. Soc. Am., 69(1), 115-133.

Mori, J., Abercrombie, R.E., 1997. Depth dependence of earthquake frequency-magnitude distributions in California: Implications for rupture initiation. J. Geophys. Res.: Solid Earth 102(B7), 15081-15090. https://doi.org/10.1029/97JB01356.

Mouthereau, F., Lacombe, O., Vergés, J., 2012. Building the Zagros collisional orogen: timing, strain distribution and the dynamics of Arabia/Eurasia plate convergence. Tectonophysics, 532, 27-60. https://doi.org/10.1016/j.tecto.2012.01.022.

Nazareth, J.J., Hauksson, E., 2004. The seismogenic thickness of the southern California crust. Bull. Seism. Soc. Am. 94(3), 940-960. https://doi.org/10.1785/0120020129.

Nocquet, J.M., 2012. Present-day kinematics of the Mediterranean: A comprehensive overview of GPS results. Tectonophysics 579, 220-242. https://doi.org/10.1016/j.tecto.2012.03.037.

Özbakır, A.D., Şengör, A.M.C., Wortel, M.J.R., Govers, R., 2013. The Pliny–Strabo trench region: a large shear zone resulting from slab tearing. Earth Planet. Sci. Lett. 375, 188-195. https://doi.org/10.1016/j.epsl.2013.05.025.

Palano, M., González, P.J., Fernández, J., 2013. Strain and stress fields along the Gibraltar Orogenic Arc: Constraints on active geodynamics. Gondwana Res. 23, 1071-1088. https://doi:10.1016/j.gr.2012.05.021.

Palano, M., Imprescia, P., Agnon, A., Gresta, S., 2018. An improved evaluation of the seismic/geodetic deformation-rate ratio for the Zagros Fold-and-Thrust collisional belt. Geophys. J. Int. 213, 194-209. https://doi:10.1093/gji/ggx524.

Palano, M., Piromallo, C., Chiarabba, C., 2017. Surface imprint of toroidal flow at retreating slab edges: The first geodetic evidence in the Calabrian subduction system. Geophys. Res. Lett. 44(2), 845-853. https://doi.org/10.1002/2016GL071452.

Palano, M., Ursino, A., Spampinato, S., Sparacino, F., Polonia, A., Gasperini, L., 2020. Crustal deformation, active tectonics and seismic potential in the Sicily Channel (Central Mediterranean), along the Nubia–Eurasia plate boundary. Sci. Rep. 10(1), 1-14. https://doi.org/10.1038/s41598-020-78063-1.

Pancha, A., Anderson, J.G., Kreemer, C., 2006. Comparison of seismic and geodetic scalar moment rates across the Basin and Range Province. Bull. Seismol. Soc. Am. 96, 11–32. https://doi.org/10.1785/0120040166.

Papazachos, C.B., Kiratzi, A.A., 1996. A detailed study of the active crustal deformation in the Aegean and surrounding area. Tectonophysics 253(1-2), 129-153. https://doi.org/10.1016/0040-1951(95)00047-X.

Papazachos, B.C., Comninakis, P.E., Scordilis, E.M., Karakaisis, G.F., Papazachos, C.B., 2010. A catalogue of earthquakes in Greece and surrounding area for the period 1901-2010. Publication of the Geophysics Laboratory, University of Thessaloniki. http://geophysics.geo.auth.gr/ss/CATALOGS/seiscat.dat; doi:10.7914/SN/HT.

Papadopoulos, G. A., 2011. A Seismic History of Crete: The Hellenic Arc and Trench. Athens.

Papanikolau, D., 2010. Major paleogeographic, tectonic and geodynamic changes from the last stage of the Hellenides to the actual Hellenic arc and trench system. Bull. Geol. Soc. Greece 43(1), 72-85. https://doi.org/10.12681/bgsg.11161.

Pérouse, E., Chamot-Rooke, N., Rabaute, A., Briole, P., Jouanne, F., Georgiev, I., Dimitrov, D., 2012. Bridging onshore and offshore present-day kinematics of central and eastern Mediterranean: implications for crustal dynamics and mantle flow. Geochem. Geophys. Geosyst. 13(9). https://doi.org/10.1029/2012GC004289.

Platt, J.P., Xia, H., Schmidt, W.L. 2018. Rheology and stress in subduction zones around the aseismic/seismic transition. Prog. Earth Planet Sci. 5, 24. https://doi.org/10.1186/s40645-018-0183-8

Rontogianni, S., 2010. Comparison of geodetic and seismic strain rates in Greece by using a uniform processing approach to campaign GPS measurements over the interval 1994-2000. J. Geodyn. 50(5), 381-399. https://doi.org/10.1016/j.jog.2010.04.008.

Rouet-Leduc, B., Jolivet, R., Dalaison, M., Johnson, P. A., Hulbert, C., 2021. Autonomous extraction of millimeter-scale deformation in InSAR time series using deep learning. Nat Commun 12, 6480. https://doi.org/10.1038/s41467-021-26254-3

Ruff, L., Kanamori, H., 1980. Seismicity and the subduction process. Phys. Earth Planet. In. 23(3), 240-252. https://doi.org/10.1016/0031-9201(80)90117-X.

Rydelek, P.A., Sacks, I.S., 1989. Testing the completeness of earthquake catalogues and the hypothesis of self-similarity. Nature 337(6204), 251-253. https://doi.org/10.1038/337251a0.

Savage, J.C., Simpson, R.W., 1997. Surface strain accumulation and the seismic moment tensor. Bull. Seismol. Soc. Am. 87, 1345-1353.

Schäfer, A.M., Wenzel, F., 2019. Global Megathrust earthquake hazard—maximum magnitude assessment using multi-variate machine learning. Front. Earth Sci. 7, 136. https://doi.org/10.3389/feart.2019.00136.

Scholz, C.H., 1968. Experimental study of the fracturing process in brittle rock. J. Geophys. Res. 73(4), 1447-1454. https://doi.org/10.1029/JB073i004p01447.

Scholz, C.H., 1998. A further note on earthquake size distributions. Bull. Seismol. Soc. Am. 88(5), 1325-1326.

Scholz, C.H., Campos, J., 2012. The seismic coupling of subduction zones revisited. J. Geophys. Res.: Solid Earth 117(B5). https://doi.org/10.1029/2011JB009003.

Şengör, A.M.C., Özeren, S., Genç, T., Zor, E., 2003. East Anatolian high plateau as a mantle-supported, north-south shortened domal structure. Geophys. Res. Lett. 30(24). https://doi.org/10.1029/2003GL017858.

Şengör, A.M.C., Tüysüz, O., Imren, C., Sakınç, M., Eyidoğan, H., Görür, N., Le Pichon, X., Rangin, C., 2005. The North Anatolian fault: A new look. Annu. Rev. Earth Planet. Sci. 33, 37-112. https://doi.org/10.1146/annurev.earth.32.101802.120415.

Şengör, A.C., Yilmaz, Y., 1981. Tethyan evolution of Turkey: a plate tectonic approach. Tectonophysics 75(3-4), 181-241. https://doi.org/10.1016/0040-1951(81)90275-4.

Senturk, S., Cakir, Z., Ergintav, S., Dogan, U., Cetin, S., Akoglu, A. M., Meghraoui, M., Karabulut, H., 2015. Surface creep along the East Anatolian fault (Turkey) revealed by InSAR time series: implications for seismic hazard and mechanism of creep. Am. Geophys. Union, Fall Meeting 2015, abstract id. G21A-1006

Reilinger, R., McClusky, S., Vernant, P., Lawrence, S., Ergintav, S., Cakmak, R., Haluk Ozener, H., Kadirov, F., Guliev, I., Stepanyan, R., Nadariya, M., Hahubia, G., Mahmoud, S., Sakr, K., ArRajehi, A., Paradissis, D., Al-Aydrus, A., Prilepin, M., Guseva, T., Evren, E., Dmitrotsa, A., Filikov, S.V., Gomez, F., Al-Ghazzi, R., Karam, G., 2006. GPS constraints on continental deformation in the Africa-Arabia-Eurasia continental collision zone and implications for the dynamics of plate interactions. J. Geophys. Res.: Solid Earth 111(B5). https://doi.org/10.1029/2005JB004051.

Shaw, B., Jackson, J., 2010. Earthquake mechanisms and active tectonics of the Hellenic subduction zone. Geophys. J. Int. 181(2), 966-984. https://doi.org/10.1111/j.1365-246X.2010.04551.x.

Shen, Z.-K., Wang, M., Zeng, Y., Wang, F., 2015. Optimal interpolation of spatially discretized geodetic data. Bull. Seismol. Soc. Am. 105, 2117–2127. https://doi:10.1785/0120140247.

Sibson, R.H., 1984. Roughness at the base of the seismogenic zone: contributing factors. J. Geophys. Res.: Solid Earth 89(B7), 5791-5799. https://doi.org/10.1029/JB089iB07p05791.

Smith-Konter, B.R., Sandwell, D.T., Shearer, P., 2011. Locking depths estimated from geodesy and seismology along the San Andreas Fault System: Implications for seismic moment release. J. Geophys. Res.: Solid Earth 116(B6). https://doi.org/10.1029/2010JB008117.

Sparacino, F., Palano, M., Peláez, J.A., Fernández, J., 2020. Geodetic deformation versus seismic crustal moment-rates: insights from the Ibero-Maghrebian region. Remote Sens. 12(6), 952. https://doi.org/10.3390/rs12060952.

Stein, R.S., 2008. Appendix D: Earthquake Rate Model 2 of the 2007 Working Group for California Earthquake Probabilities, Magnitude Area Relationships. U.S. Geol. Surv. Open File Rep. 2007, 1437D, 1– 16.

Stevens, V. L., Avouac, J. P., 2021. On the relationship between strain rate and seismicity in the India-Asia collision zone: implications for probabilistic seismic hazard. Geophys. J. Int. 226(1), 220-245. https://doi.org/10.1093/gji/ggab098.

Stucchi, M., Rovida, A., Capera, A.G., Alexandre, P., Camelbeeck, T., Demircioglu, M.B., Gasperini, P., Kouskouna, V., Musson, R.M.W., Radulian, M., Sesetyan, K., Vilanova, S., Baumont, D., Bungum, H., Fäh, D., Lenhardt, W., Makropoulos, K., Martinez Solares, J.M., Scotti, O., Živčić, M., Albini, P., Batllo, J., Papaioannou, C., Tatevossian, R., Locati, M., Meletti, C., Viganò, D., Giardini, D., 2013. The SHARE European earthquake catalogue (SHEEC) 1000–1899. J. Seismolog. 17(2), 523-544. https://doi.org/10.1007/s10950-012-9335-2.

Tatar, O., Poyraz, F., Gürsoy, H., Cakir, Z., Ergintav, S., Akpınar, Z., Koçbulut, F., Sezen, F., Türk, T., Hastaoğlu, K.Ö., Polat, A., Levent Mesci, B., Gürsoy, Ö., Ayazlı, E., Çakmak, R., Belgen, A., Yavaşoğlu, H., 2012. Crustal deformation and kinematics of the Eastern Part of the North Anatolian Fault Zone (Turkey) from GPS measurements. Tectonophysics 518, 55-62. https://doi.org/10.1016/j.tecto.2011.11.010.

The European Database of Seismogenic Faults (EDSF). http://diss.rm.ingv.it/share-edsf (accessed 19 July 2021).

The SHARE European Earthquake Catalogue. https://www.emidius.eu/SHEEC (accessed on 19 July 2021).

Tiryakioğlu, İ., Floyd, M., Erdoğan, S., Gülal, E., Ergintav, S., McClusky, S., Reilinger, R., 2013. GPS constraints on active deformation in the Isparta Angle region of SW Turkey. Geophys. J. Int. 195(3), 1455-1463. https://doi.org/10.1093/gji/ggt323.

TSUMAPS NEAM - Probabilistic Tsunami Hazard Maps for the Neam Region. http://www.tsumaps-neam.eu (accessed on 19 July 2021).

Turcotte, D., Schubert, G., 2002. Geodynamics, Cambridge University Press: Cambridge, UK.

Uyeda, S., 1982. Subduction zones: an introduction to comparative subductology. Tectonophysics 81(3-4), 133-159. https://doi.org/10.1016/0040-1951(82)90126-3.

van Hinsbergen, D.J.J., Torsvik, T.H., Schmid, S.M., Maţenco, L.C., Maffione, M., Vissers, R.L.M., Gürer, D., Spakman, W., 2020. Orogenic architecture of the Mediterranean region and kinematic

reconstruction of its tectonic evolution since the Triassic. Gondwana Res. 81, 79-229, ISSN 1342-937X. https://doi.org/10.1016/j.gr.2019.07.009.

Vernant, P., Reilinger, R., McClusky, S., 2014. Geodetic evidence for low coupling on the Hellenic subduction plate interface. Earth Planet. Sci. Lett. 385, 122-129. https://doi.org/10.1016/j.epsl.2013.10.018.

Visini, F., et al., 2021. Earthquake Rupture Forecasts for the MPS19 Seismic Hazard Model of Italy. Ann. Geophys. 64(2), SE220. https://doi.org/10.4401/ag-8608.

Wang, L., Wang, R., Roth, F., Enescu, B., Hainzl, S., Ergintav, S., 2009. Afterslip and viscoelastic relaxation following the 1999 M 7.4 Izmit earthquake from GPS measurements. Geophys. J. Int. 178(3), 1220-1237. https://doi.org/10.1111/j.1365-246X.2009.04228.x.

Ward, S.N., 1998. On the consistency of earthquake moment rates, geological fault data, and space geodetic strain: The United States. Geophys. J. Int. 134, 172–186. https://doi:10.1046/j.1365-246x.1998.00556.x.

Wdowinski, S., Ben-Avraham, Z., Arvidsson, R., Ekström, G., 2006. Seismotectonics of the Cyprian arc. Geophys. J. Int. 164(1), 176-181. https://doi.org/10.1111/j.1365-246X.2005.02737.x.

Weichert, D.H., 1980. Estimation of the earthquake recurrence parameters for unequal observation observation periods for different magnitudes. Bull. Seismol. Soc. Am. 70, 1337–1346. https://doi.org/10.1785/BSSA0700041337.

Weiss, J.R., Walters, R.J., Morishita, Y., Wright, T.J., Lazecky, M., Wang, H., Hussain, E., Hooper, A.J., Elliott, J.R., Rollins, C., Yu, C., González, P.J., Spaans, K., Li, Z., Parsons, B., 2020. High-resolution surface velocities and strain for Anatolia from Sentinel-1 InSAR and GNSS data. Geophys. Res. Lett. 47(17). https://doi.org/10.1029/2020GL087376.

Wells, D.L., Coppersmith, K.J., 1994. New empirical relationship among magnitude, rupture length, rupture width, rupture area, and surface displacement. Bull. Seismol. Soc. Am. 84, 974–1002.

Wiemer, S., Wyss, M., 2000. Minimum magnitude of completeness in earthquake catalogs: examples from Alaska, the western United States, and Japan. Bull. Seism. Soc. Am. 90(4), 859–869. https://doi.org/10.1785/0119990114.

Williams, C.F., 1996. Temperature and the seismic/aseismic transition: Observations from the 1992 Landers earthquake. Geophys. Res. Lett. 23(16), 2029-2032. https://doi.org/10.1029/96GL02066.

Woessner, J., Danciu L., D. Giardini and the SHARE consortium, 2015. The 2013 European Seismic Hazard Model: key components and results. Bull. Earthq. Eng. 13, 3553-3596. https://doi.org/10.1007/s10518-015-9795-1.

Yolsal-Cevikbilen, S., Biryol, C.B., Beck, S., Zandt, G., Taymaz, T., Adiyaman, H.E., Özacar, A.A., 2012. 3-D crustal structure along the North Anatolian Fault Zone in north-central Anatolia revealed by local earthquake tomography. Geophys. J. Int. 188(3), 819-849. https://doi.org/10.1111/j.1365-246X.2011.05313.x.